12

Fragmentation functions: e^+e^- annihilation to hadrons, and SIDIS

We now extend our treatment of factorization to cover the distribution of final-state hadrons in hard processes.

The simplest process is the cross section for inclusive one-hadron production in e^+e^- annihilation, Fig. 12.1,

$$e^+e^- \to \gamma^*(q) \to h(p) + X, \tag{12.1}$$

where the hadron is typically a pion, and, as usual, we work to lowest order in electroweak interactions. Kinematically the process is the same as inclusive DIS, except that certain particles are crossed between the initial and final states. We will see that the *structure* of the factorization theorem, (12.21), is the same as for DIS. The differences concern the time ordering of the process: the hard scattering is for a virtual photon to make a partonic state from a highly virtual time-like photon of momentum q. The place of a parton density is taken by a new object, called a fragmentation function; it represents the distribution of the final-state detected hadron resulting from an outgoing parton that originated in the hard scattering.

Our proof of factorization will introduce two important conceptual changes relative to DIS. The first is that we need a more detailed examination of soft gluon effects before we prove they cancel. This is because the detected hadron in the final state prevents the transition to an uncut amplitude that we used for DIS in Sec. 11.2. We will first use Ward identities to factorize the soft part, as we did for the Sudakov form factor in Ch. 10. Only after that can we employ the sum-over-cuts argument to obtain cancellation.

The second change relative to DIS arises from an issue we discussed in Ch. 4 that concerns final-state interactions. Our proof of factorization relies on the structure of leading regions as seen in Feynman graphs, which also correspond to certain regions in space-time. For our arguments to apply to full QCD, we need to assume that these regions are also correct after non-perturbative effects are included.

We will need to make the assumption that the "breakable string" picture of hadronization rather than the "unbreakable elastic spring" applies to QCD; see Sec. 4.3.1. (Of course our arguments would also apply if quarks and gluons were unconfined.) This assumption is abundantly supported by experimental data, but it is not (yet) derived from QCD. Associated with this will be a notable jump in the logic of the derivation.
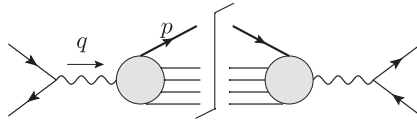
Fig. 12.1. Cross section for $e^+e^- \to h(p) + X$.

If, instead, the unbreakable spring picture had been correct, then the partonic state from the hard scattering would first form a resonance. In this case there would be no necessary correspondence between the directions of the decay products and of the partons, contrary to the measured situation with QCD jet physics.

For the DIS structure functions we evaded these issues by treating the *uncut* amplitude $T^{\mu\nu}$. But this option is no longer available to us now that we have a detected hadron in the final state.

After our treatment for the single-hadron-inclusive cross section in e^+e^- annihilation, we will have the methods necessary to treat other reactions. For example, factorization and its proof can readily be generalized to inclusive cross sections with more than one detected hadron. Another case is semi-inclusive deeply inelastic scattering (SIDIS). This is a cross section for DIS in which one (or more) particles is detected in the final state. The label SIDIS is generally applied to single particle production,

$$e + P \to e + \pi(p_B) + X, \tag{12.2}$$

although the same ideas apply to more general cases.

12.1 Structure-function analysis of one-particle inclusive cross section

12.1.1 Hadronic tensor

As with DIS, the squared amplitude for our process, Fig. 12.1, factorizes into a leptonic and a hadronic part. We use a structure-function analysis (Drell, Levy, and Yan, 1970) for the hadronic tensor, which is defined by

$$W^{\mu\nu}(q, p) \stackrel{\text{def}}{=} 4\pi^3 \sum_X \delta^{(4)}(p_X + p - q) \langle 0|j^\mu(0)|p, X, \text{ out}\rangle \langle p, X, \text{ out}|j^\nu(0)|0\rangle$$

$$= \frac{1}{4\pi} \sum_X \int \mathrm{d}^4 z \; e^{iq \cdot z} \langle 0|j^\mu(z/2)|p, X, \text{ out}\rangle \langle p, X, \text{ out}|j^\nu(-z/2)|0\rangle . \tag{12.3}$$

The primary difference compared with DIS is that the selected hadron is in the final state, so we cannot eliminate the $\sum_X$ as we did for DIS in (2.18), and we need to explicitly indicate that the states are out-states. The photon momentum q is now time-like. Our normalization conventions, both for the states and for $W^{\mu\nu}$, differ from those of Drell, Levy, and Yan (1970).

We define $Q = \sqrt{q^2}$, and we define the equivalent of the Bjorken variable by

$$x = 2p \cdot q/Q^2. \tag{12.4}$$

We interpret x as the center-of-mass energy of the detected particle relative to its maximum value $Q/2$ (when masses are neglected). The decomposition into structure functions is

$$W^{\mu\nu} = \left(-g^{\mu\nu} + \frac{q^\mu q^\nu}{q^2}\right) F_1(x, Q^2) + \frac{\left(p^\mu - \frac{q^\mu p \cdot q}{q^2}\right)\left(p^\nu - \frac{q^\nu p \cdot q}{q^2}\right)}{p \cdot q} F_2(x, Q^2), \quad (12.5)$$

which assumes current conservation, parity invariance, and that the detected hadron is either spinless or has its polarization states summed over. An F_3 structure function [cf. (7.3)] is needed if Z boson exchange is included, since then parity is violated.

The inclusive cross section is

$$E\frac{d\sigma}{d^3 p} = \frac{2\alpha^2}{Q^6} L_{\mu\nu} W^{\mu\nu}, \quad (12.6)$$

where the leptonic tensor is

$$L^{\mu\nu} = l_1^\mu l_2^\nu + l_2^\mu l_1^\nu - g^{\mu\nu} l_1 \cdot l_2, \quad (12.7)$$

where l_1 and l_2 are the momenta of the incoming electron and positron, and where the electron mass is neglected. Hence

$$E\frac{d\sigma}{d^3 p} = \frac{2\alpha^2}{Q^4}\sqrt{1 - \frac{4m^2}{Q^2 x^2}}\left[F_1(x, Q) + \frac{x}{4}\left(1 - \frac{4m^2}{Q^2 x^2}\right)\sin^2\theta F_2(x, Q)\right]$$

$$\simeq \frac{2\alpha^2}{Q^4}\left[F_1(x, Q) + \frac{x}{4}\sin^2\theta F_2(x, Q)\right]. \quad (12.8)$$

Here, m is the mass of the detected hadron, and θ is its angle relative to the electron in the center-of-mass frame. In the last line, m was neglected.

A standard presentation is

$$\frac{d\sigma}{dx\, d\cos\theta} = \frac{3}{8}(1 + \cos^2\theta)\frac{d\sigma_T}{dx} + \frac{3}{4}\sin^2\theta\frac{d\sigma_L}{dx}, \quad (12.9)$$

where

$$\frac{d\sigma_T}{dx} = \frac{4\pi\alpha^2}{3Q^2}x F_1(x, Q), \quad (12.10a)$$

$$\frac{d\sigma_L}{dx} = \frac{\pi\alpha^2}{3Q^2}\left[2x F_1(x, Q) + x^2 F_2(x, Q)\right]. \quad (12.10b)$$

12.1.2 Averaging with test function

To derive factorization, we will use certain cancellations generalizing those we saw in Sec. 4.1.1, for the total cross section for $e^+ e^- \to$ hadrons, and in Sec. 11.2.1, for DIS. The cancellations involve terms that differ by whether particular lines are real or virtual, and thus by change of final state. The proof is clearest if a loop integral involving the momentum of a particular final-state particle can be routed out through the current vertex rather than back through other final-state particles. This can be done by averaging the hadronic tensor

with a test function $f(q)$:

$$W^{\mu\nu}([f], p) \overset{\text{def}}{=} \int \mathrm{d}^4 q\, f(q)\, W^{\mu\nu}(q, p)$$

$$= 4\pi^3 \sum_X f(p_X + p)\, \langle 0|j^{\mu}(0)|p, X, \text{ out}\rangle\, \langle p, X, \text{ out}|j^{\nu}(0)|0\rangle\,. \quad (12.11)$$

Here, the square brackets in $[f]$ act as a reminder that the argument is a whole function, and not just its value at one point. The integral over q has removed the momentum-conservation delta function from (12.3), and therefore allows the desired routing of integrals of final-state momenta.

The actual hadronic tensor is obtained by functional differentiation:

$$W^{\mu\nu}(q, p) = \frac{\delta W^{\mu\nu}([f], p)}{\delta f(q)}. \quad (12.12)$$

But the derivation of factorization only applies when the test function has a suitably slow dependence on Q, so that factorization generally only applies to a locally averaged quantity. If the actual hadronic tensor has smooth dependence on kinematic variables, the local average is unnecessary.

12.2 Statement of factorization etc. for $e^+e^- \to h(p) + X$

I now state the main results for factorization and fragmentation function evolution, all to be derived in later sections.

12.2.1 Factorization for cross section

The factorized cross section has the form

$$E \frac{\mathrm{d}\sigma(e^+e^- \to h(p) + X)}{\mathrm{d}^3 \boldsymbol{p}} = \sum_j \int_{x-}^{1+} \frac{\mathrm{d}z}{z^2}\, E_k \frac{\mathrm{d}\hat{\sigma}_j}{\mathrm{d}^3 \boldsymbol{k}}\, d_{h/j}(z; \mu). \quad (12.13)$$

As usual, this formula is valid up to corrections suppressed by a power of $1/Q$. We use $\mathrm{d}\hat{\sigma}_j$ to denote the perturbatively calculable hard-scattering factor, normalized like the differential cross section for inclusive production of an on-shell massless parton of type j and 3-momentum $\boldsymbol{k}$. Like the hard scattering in DIS, it must contain subtractions to prevent double counting between momentum regions. The 3-momenta, $\boldsymbol{p}$ and $\boldsymbol{k}$, of the hadron and parton are made parallel in the overall center-of-mass frame, with a ratio z: $\boldsymbol{p} = z\boldsymbol{k}$.

The quantity $d_{h/j}(z; \mu)$ is the fragmentation function, whose exact definition we will give later; we approximate its meaning as the number density to find hadron h in the jet initiated by parton j, with the hadron having a fraction z of the parton's momentum. The reality of the jets is evidenced by pictures like Fig. 5.10, which shows an event in DIS.

As with parton densities, this intuitive meaning only applies literally in a super-renormalizable non-gauge theory. After applying correct definitions and derivations in
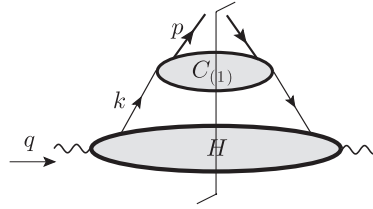
Fig. 12.2. Structure of factorization for one-hadron-inclusive cross section in e^+e^- annihilation.

QCD, the factorization formula will remain correct, but the number/probability interpretation will not be really correct. As with parton densities, there is a DGLAP evolution equation for the fragmentation function. It lets us set the scale μ of the fragmentation functions to be of order the experimentally dependent quantity Q, so that the hard scattering is calculable in fixed-order perturbation theory.

The factor $1/z^2$ in (12.13) arises because of the change of variable between the hadron momentum on the l.h.s. and the parton momentum on the r.h.s.: with neglect of masses $\mathrm{d}^3\boldsymbol{p}/E_{\boldsymbol{p}} = z^2\,\mathrm{d}^3\boldsymbol{k}/E_{\boldsymbol{k}}$. If we were to use n space-time dimensions, the factor $1/z^2$ would be replaced by $1/z^{n-2}$.

The structure of factorization is illustrated in Fig. 12.2. The hard scattering H makes two or more final-state partons. One of these of momentum k goes into the fragmentation subgraph, which is labeled $C_{(1)}$ to be consistent with a notation used later. The details of the proof of factorization will show that Fig. 12.2 is misleadingly simple. There will be non-trivial cancellations to be proved before we obtain the factorized structure. The figure also omits reference to the Wilson lines in the definitions of the fragmentation functions.

Where fragmentation functions get used

The most basic situation for using a fragmentation function is the one-hadron-inclusive cross section in e^+e^- annihilation, just described.

Straightforward generalizations of the factorization theorem apply to semi-inclusive DIS (e.g., $e + p \to e + \pi + X$), to multiple hadron production in e^+e^- annihilation, and to production of hadrons of high transverse momentum in hadron-hadron collisions. All of these factorization theorems use fragmentation functions for the detected final-state hadrons; the same fragmentation functions for all these processes. Global fits have been performed in de Florian, Sassot, and Stratmann (2007); Albino, Kniehl, and Kramer (2008).

Terminology

The Particle Data Group (Amsler *et al.*, 2008, p. 202) uses the term "fragmentation function" to refer to both a partonic fragmentation function, as in (12.13), and to the following normalized cross section:

$$F^h(x, Q^2) = \frac{1}{\sigma_{\mathrm{tot}}}\frac{\mathrm{d}\sigma}{\mathrm{d}x}(e^+e^- \to hX). \tag{12.14}$$

I find it preferable to distinguish these concepts, for the same reasons that the concepts of "structure function" and "parton density" should be distinguished in DIS. So I only use "fragmentation function" to refer to a partonic fragmentation function.

12.2.2 Renormalization and DGLAP evolution of fragmentation functions

As in the case of parton densities, the basic definitions of fragmentation functions have UV divergences. The factorization formula uses renormalized fragmentation functions obtained from bare fragmentation functions by formulae of the form

$$d_{h/j}(z; \mu) = \lim_{\epsilon \to 0} \sum_{j'} \int_{z-}^{1+} \frac{\mathrm{d}\rho}{\rho}\, d_{(0)\, h/j'}(z/\rho)\, L_{j'j}(\rho; g(\mu), \epsilon). \tag{12.15}$$

(Here, as usual $\epsilon = 2 - n/2$, where n is the space-time dimension.)

There follow DGLAP evolution equations, of the same form (8.30) as for parton densities:

$$\frac{\mathrm{d}}{\mathrm{d}\ln\mu} d_{h/j}(z; \mu) = 2 \sum_{j'} \int_{z-}^{1+} \frac{\mathrm{d}\rho}{\rho}\, d_{h/j'}(z/\rho; \mu)\, P_{j'j}(\rho; g(\mu)). \tag{12.16}$$

See Sec. 12.10 below for a calculation that shows the LO kernels have the same value as for parton densities. The finite evolution kernels are obtained from the renormalization factors:

$$\frac{\mathrm{d}}{\mathrm{d}\ln\mu} L_{j'j}(\rho; g(\mu), \epsilon) = 2 \sum_{j''} \int \frac{\mathrm{d}\rho'}{\rho'}\, L_{j'j''}(\rho/\rho'; g, \epsilon)\, P_{j''j}(\rho'; g, \epsilon). \tag{12.17}$$

Just as with parton densities, the convolutions in the above equations turn into multiplications for moments. Let us define

$$\tilde{d}_{h/j}(n; \mu) = \int_0^1 \mathrm{d}z\, z^{n-1} d_{h/j}(z; \mu), \quad \tilde{L}_{j'j}(n; \mu) = \int_0^1 \mathrm{d}\rho\, \rho^{n-1} L_{j'j}(\rho; \mu), \tag{12.18}$$

etc. Then the renormalization and DGLAP equations are

$$\tilde{d}_{h/j}(n; \mu) = \lim_{\epsilon \to 0} \sum_{j'} \tilde{d}_{(0)\, h/j'}(n)\, \tilde{L}_{j'j}(n; g(\mu), \epsilon), \tag{12.19}$$

$$\frac{\mathrm{d}}{\mathrm{d}\ln\mu} \tilde{d}_{h/j}(n; \mu) = 2 \sum_{j'} \tilde{d}_{h/j'}(n; \mu)\, \tilde{P}_{j'j}(n; g(\mu)). \tag{12.20}$$

12.2.3 Factorization for hadronic tensor

We convert (12.13) to a factorization for $W^{\mu\nu}$:

$$W^{\mu\nu}(p, q) = \sum_{j} \int_{x-}^{1+} \frac{\mathrm{d}z}{z^2}\, d_{h/j}(z; \mu)\, C_j^{\mu\nu}(\hat{k}, q; g(\mu), \mu). \tag{12.21}$$

The hard-scattering tensor $C_j^{\mu\nu}$ is just like $W^{\mu\nu}$, except that it is at the partonic level, and is defined with double-counting subtractions to remove non-short-distance contributions.
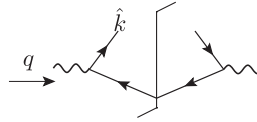
Fig. 12.3. Lowest-order partonic graph for $e^+e^- \to \text{quark}_j(\hat{k}) + X$.

It uses an approximated parton momentum

$$\hat{k} = (p^+/z, 0, \mathbf{0}_{\mathrm{T}}), \tag{12.22}$$

where we use light-front coordinates such that $p = (p^+, m^2/2p^+, \mathbf{0}_{\mathrm{T}})$.

12.2.4 Projection onto structure functions

We define partonic structure functions $\hat{F}_{ij}$ by applying (12.5) to $C_j^{\mu\nu}$:

$$C_j^{\mu\nu} = \left(-g^{\mu\nu} + \frac{q^\mu q^\nu}{q^2}\right) \hat{F}_{1j}(x/z, Q^2) + \frac{\left(\hat{k}^\mu - \frac{q^\mu \hat{k}\cdot q}{q^2}\right)\left(\hat{k}^\nu - \frac{q^\nu \hat{k}\cdot q}{q^2}\right)}{\hat{k}\cdot q} \hat{F}_{2j}(x/z, Q^2). \tag{12.23}$$

Hence we get factorization formulae for the structure functions:

$$F_1(x, Q^2) = \sum_j \int_{x-}^{1+} \frac{\mathrm{d}z}{z^2} \, d_{h/j}(z; \mu) \, \hat{F}_{1j}(x/z, Q^2), \tag{12.24a}$$

$$F_2(x, Q^2) = \sum_j \int_{x-}^{1+} \frac{\mathrm{d}z}{z^3} \, d_{h/j}(z; \mu) \, \hat{F}_{2j}(x/z, Q^2), \tag{12.24b}$$

and similarly for the transverse and longitudinal cross sections:

$$\frac{\mathrm{d}\sigma_T}{\mathrm{d}x} = \sum_j \int_{x-}^{1+} \frac{\mathrm{d}z}{z} \, d_{h/j}(z; \mu) \frac{\mathrm{d}\hat{\sigma}_{T,j}(x/z)}{\mathrm{d}(x/z)}, \tag{12.25a}$$

$$\frac{\mathrm{d}\sigma_L}{\mathrm{d}x} = \sum_j \int_{x-}^{1+} \frac{\mathrm{d}z}{z} \, d_{h/j}(z; \mu) \frac{\mathrm{d}\hat{\sigma}_{L,j}(x/z)}{\mathrm{d}(x/z)}. \tag{12.25b}$$

12.3 LO calculation

Even without a proof of factorization we can see how to get the lowest order of the hard scattering. As in DIS, we just need the LO calculation of one-parton-inclusive scattering, from the graph of Fig. 12.3:

$$\begin{aligned} C_j^{\mu\nu} &= \frac{e_j^2 N_c}{4\pi} \int \frac{\mathrm{d}^3 \mathbf{k}_2}{(2\pi)^3 2|\mathbf{k}_2|} (2\pi)^4 \delta^{(4)}(q - \hat{k} - k_2) \operatorname{Tr} \gamma^\mu \hat{\slashed{k}} \gamma^\nu \slashed{k}_2 \\ &= e_j^2 N_c \delta(x/z - 1) \left[-g^{\mu\nu} - \frac{2}{Q^2}(2\hat{k}^\mu \hat{k}^\mu - q^\mu \hat{k}^\nu - \hat{k}^\mu q^\nu) \right]. \end{aligned} \tag{12.26}$$

We have included a factor N_c, since we always sum over parton color in the final state. (The fragmentation function will have a color average.) In the first line, we integrate over the momentum k_2 of what we can term the unobserved parton, the one not associated with the observed hadron. In the calculation of the hard scattering the external partons are set on-shell, whereas the actual parton momenta are off-shell. In particular, $\hat{k}$ denotes the approximated on-shell momentum given in (12.22).

We deduce the partonic structure functions

$$\hat{F}_{1j} = e_j^2 N_c \delta(x/z - 1) + O(\alpha_s), \quad \hat{F}_{2j} = -2e_j^2 N_c \delta(x/z - 1) + O(\alpha_s), \quad (12.27)$$

which apply to both quarks and antiquarks.

From the factorization formula, we deduce that at the hadronic level

$$F_1 = \frac{1}{x} \sum_{\text{quarks } j} e_j^2 N_c \left(d_{h/j}(x) + d_{h/\bar{j}}(x) \right) + O(\alpha_s), \quad (12.28a)$$

$$F_2 = \frac{-2}{x^2} \sum_{\text{quarks } j} e_j^2 N_c \left(d_{h/j}(x) + d_{h/\bar{j}}(x) \right) + O(\alpha_s). \quad (12.28b)$$

We see that at lowest order an analog of the Callan-Gross relation applies: $F_2 = -2x^{-1}F_1$. Therefore the angular distribution of the hadron is given by the same $1 + \cos^2 \theta$ factor as for the elementary $e^+e^- \to q\bar{q}$ process:

$$E\frac{\mathrm{d}\sigma}{\mathrm{d}^3 \boldsymbol{p}} = \frac{\alpha^2}{Q^4 x}(1 + \cos^2 \theta) \sum_{\text{quarks } j} e_j^2 N_c \left(d_{h/j}(x) + d_{h/\bar{j}}(x) \right) + O(\alpha_s). \quad (12.29)$$

From the inclusive cross section formula (12.8) and the total cross section formulae in Sec. 4.1, we find that the normalized distribution in x directly reflects the values of the fragmentation functions, weighted by quark charge squared:

$$\frac{\mathrm{d}\sigma(e^+e^- \to hX)/\mathrm{d}x}{\sigma(e^+e^- \to \text{hadrons})} = \frac{\sum_{\text{quarks } j} e_j^2 \left(d_{h/j}(x) + d_{h/\bar{j}}(x) \right)}{\sum_{\text{quarks } j} e_j^2} + O(\alpha_s). \quad (12.30)$$

12.4 Introduction to fragmentation functions

The intuitive idea of a fragmentation function to represent the number density for hadrons in the jet induced by a parton is quite natural. Light-front quantization, which we studied in Sec. 6.6, gives a natural first attempt at a formal definition of fragmentation functions that directly implements the desired distribution. We now present these definitions, which are quite simple. They provide an orientation for the more complicated results in QCD.

Since the number interpretation depends on the use of the canonical commutation relations for bare fields, the definitions in this section are for bare fragmentation functions. Bare quantities are denoted by a subscript "(0)". For a statement of the renormalization properties, see Sec. 12.2.2.

12.4.1 Kinematics

Our implementation uses two different coordinate frames, called the hadron and parton frames, with components denoted by subscripts h and p respectively. Thus for a vector V, we write

$$V_h = \left(V_h^+, V_h^-, \boldsymbol{P}_{h\,\mathrm{T}}\right), \quad V_p = \left(V_p^+, V_p^-, \boldsymbol{P}_{p\,\mathrm{T}}\right), \tag{12.31}$$

in the hadron and parton frames. We will arrange that the plus components are the same in both frames, so that for this component we can drop the frame's subscripts: $V_h^+ = V_p^+ = V^+$.

The hadron frame is the one already used where the detected hadron has zero transverse momentum: $p_h = \left(p^+, m^2/(2p^+), \boldsymbol{0}_{\mathrm{T}}\right)$. The actual parton momentum, as in Fig. 12.2, has non-zero transverse momentum:

$$k_h = \left(k^+, k_h^-, \boldsymbol{k}_{h\,\mathrm{T}}\right) = \left(p^+/z, k_h^-, \boldsymbol{k}_{h\,\mathrm{T}}\right). \tag{12.32}$$

Of course, the approximated parton has zero transverse momentum: $\hat{k}_h = (k^+, 0, \boldsymbol{0}_{\mathrm{T}}) = (p^+/z, 0, \boldsymbol{0}_{\mathrm{T}})$.

For defining the number density of hadrons in the jet induced by a parton of momentum k, we need a frame in which it is the parton that has zero transverse momentum, and the hadron has non-zero transverse momentum. For this we use the parton frame, defined to be obtained from the hadron frame by the following Lorentz transformation:

$$V_p^+ = V_h^+,$$
$$V_p^- = \frac{k_{h\,\mathrm{T}}^2}{2(k^+)^2} V_h^+ + V_h^- - \frac{\boldsymbol{k}_{h\,\mathrm{T}}}{k^+} \cdot \boldsymbol{V}_{h\,\mathrm{T}}, \tag{12.33}$$
$$\boldsymbol{V}_{p\,\mathrm{T}} = -\frac{\boldsymbol{k}_{h\,\mathrm{T}}}{k^+} V_h^+ + \boldsymbol{V}_{h\,\mathrm{T}},$$

a Lorentz transformation that changes as k varies. Hence the parton-frame components are

$$k_p = \left(k^+, k_p^-, \boldsymbol{0}_{\mathrm{T}}\right) = \left(k^+, k_h^- - k_{h\,\mathrm{T}}^2/(2k^+), \boldsymbol{0}_{\mathrm{T}}\right), \tag{12.34a}$$

$$p_p = \left(zk^+, \frac{m^2 + k_{h\,\mathrm{T}}^2 z^2}{2zk^+}, -z\boldsymbol{k}_{h\,\mathrm{T}}\right). \tag{12.34b}$$

Note carefully the factor of z and the reversed sign between the parton transverse momentum in the one frame and the hadron transverse momentum in the other frame.

Although the parton frame is a natural one for defining fragmentation functions as number densities, it is inconvenient for derivations of factorization. The problem is that, in a physical process, there is an integral over parton momentum, and so the parton-frame axes are not fixed. Neither parton momenta nor the resulting parton-frame axes can be determined from experimentally measured quantities. Therefore we will express the definitions of fragmentation functions in hadron-frame coordinates. In the derivation of factorization, we will use a hadron frame defined in terms of measured quantities.

12.4.2 General definition of fragmentation function

We define the fragmentation function as the number density for finding a hadron of flavor h in a parton of flavor j, given the hadron's fractional plus momentum, and its transverse momentum:

$$
\begin{aligned}
d_{(0)\,h/j}(z, \boldsymbol{p}_{p\,\mathrm{T}}) \, \langle j; k_1 | j; k_2 \rangle &\overset{\text{def}}{=} \frac{\mathrm{Tr}_{\text{color}}}{N_{c,j}} \, \langle j; k_1 | j; k_2 \rangle \, \frac{\mathrm{d}N_{j/h}}{\mathrm{d}z\, \mathrm{d}^{n-2}\boldsymbol{p}_{p\,\mathrm{T}}} \\
&= \frac{\mathrm{Tr}_{\text{color}}}{N_{c,j}} \frac{1}{2z(2\pi)^{n-1}} \sum_X \langle j, k_1 | p, X, \text{ out} \rangle \, \langle p, X, \text{ out} | j, k_2 \rangle \, .
\end{aligned}
$$

(12.35)

Here $|j, k_1\rangle$ denotes a partonic state created by a light-front creation operator, i.e., $a^{\dagger}_{j, k^{+}_{1,p}, \boldsymbol{k}_{1,p\mathrm{T}}} |0\rangle$. A number density is obtained from matrix elements of normalized states for partons and hadrons. Since we wish to use momentum eigenstates, we bring in an off-diagonal matrix element in (12.35). To cover the generalization to QCD, we define the fragmentation function to include an average over parton color. We let $N_{c,j}$ be the number of colors for field ϕ_j; in QCD it is 3 for a quark and 8 for a gluon. Then the color average is implemented as $1/N_{c,j}$ times a trace over color indices for the parton.
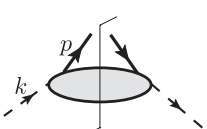
Next we use formulae like (6.64a) to express the annihilation and creation operators in terms of fields, and use methods similar to those used for the pdf in Sec. 6.7.3.

12.4.3 Scalar quark

For a scalar quark we get

$$
\begin{aligned}
d_{(0)\,h/j}(z, \boldsymbol{p}_{p\,\mathrm{T}}) &= \frac{\mathrm{Tr}_{\text{color}}}{N_{c,j}} \sum_X \frac{k^+}{z} \int \frac{\mathrm{d}x_p^- \, \mathrm{d}^{n-2}\boldsymbol{x}_{p\,\mathrm{T}}}{(2\pi)^{n-1}} e^{ik^+ x_p^-} \\
&\quad \times \langle 0 | \phi_j^{(0)}(x/2) | p, X, \text{ out} \rangle \, \langle p, X, \text{ out} | \phi_j^{(0)}(-x/2)^{\dagger} | 0 \rangle \, ,
\end{aligned}
$$

(12.36)

where $x_p = (0, x_p^-, \boldsymbol{x}_{p\,\mathrm{T}})$. In the hadron frame, we get

$$
\begin{aligned}
d_{(0)\,h/j}(z, -z\boldsymbol{k}_{h\,\mathrm{T}}) &= \frac{\mathrm{Tr}_{\text{color}}}{N_{c,j}} \sum_X \frac{k^+}{z} \int \frac{\mathrm{d}x_h^- \, \mathrm{d}^{n-2}\boldsymbol{x}_{h\,\mathrm{T}}}{(2\pi)^{n-1}} e^{ik^+ x_h^- - i\boldsymbol{k}_{h\,\mathrm{T}}\cdot\boldsymbol{x}_{h\,\mathrm{T}}} \\
&\quad \times \langle 0 | \phi_j^{(0)}(x/2) | p, X, \text{ out} \rangle \, \langle p, X, \text{ out} | \phi_j^{(0)}(-x/2)^{\dagger} | 0 \rangle \\
&= \frac{\mathrm{Tr}_{\text{color}}}{N_{c,j}} \frac{k^+}{z} \int \frac{\mathrm{d}k_h^-}{(2\pi)^n} \quad
\end{aligned}
$$

(12.37)

where the vector x has hadron-frame components $x_h = (0, x_h^-, \boldsymbol{x}_{h\,\mathrm{T}})$. The integrated fragmentation function is

$$
\begin{aligned}
d_{(0)\,h/j}(z) &\stackrel{\text{def}}{=} \int \mathrm{d}^{n-2} \boldsymbol{p}_{p\,\mathrm{T}}\, d_{h/j}(z, \boldsymbol{p}_{p\,\mathrm{T}}) \\
&= \frac{\mathrm{Tr}_{\mathrm{color}}}{N_{c,j}} \sum_X k^+ z^{n-3} \int \frac{\mathrm{d}x_h^-}{2\pi} e^{ik^+ x_h^-} \\
&\qquad \times \langle 0 | \phi_j^{(0)}(x/2) | p, X, \mathrm{out} \rangle \langle p, X, \mathrm{out} | \phi_j^{(0)}(-x/2)^\dagger | 0 \rangle \\
&= \frac{\mathrm{Tr}_{\mathrm{color}}}{N_{c,j}} k^+ z^{n-3} \int \frac{\mathrm{d}k_h^-\, \mathrm{d}^{n-2}\boldsymbol{k}_{h\,\mathrm{T}}}{(2\pi)^n} \quad k
\end{aligned}
\tag{12.38}
$$

where now $x_h = (0, x_h^-, \boldsymbol{0}_{\mathrm{T}})$. The factor z^{n-3} is perhaps unexpected, given the corresponding formula (6.124) for a parton density. It arises from the normalization of the hadron state, and then from the change of variable from the parton to the hadron frame.

12.4.4 Unpolarized Dirac quark

For a Dirac field, the derivations are readily modified to give

$$
\begin{aligned}
d_{(0)\,h/j}(z, \boldsymbol{p}_{p\,\mathrm{T}}) &= \frac{\mathrm{Tr}_{\mathrm{color}}}{N_{c,j}} \frac{\mathrm{Tr}_{\mathrm{Dirac}}}{4} \sum_X \frac{1}{z} \int \frac{\mathrm{d}x_h^-\, \mathrm{d}^{n-2}\boldsymbol{x}_{h\,\mathrm{T}}}{(2\pi)^{n-1}} e^{ik^+ x_h^- - i\boldsymbol{k}_{\mathrm{T}} \cdot \boldsymbol{x}_{h\,\mathrm{T}}} \\
&\qquad \times \langle 0 | \gamma^+ \psi_j^{(0)}(x/2) | p, X, \mathrm{out} \rangle \langle p, X, \mathrm{out} | \bar{\psi}_j^{(0)}(-x/2) | 0 \rangle \\
&= \frac{\mathrm{Tr}_{\mathrm{color}}}{N_{c,j}} \frac{\mathrm{Tr}_{\mathrm{Dirac}}}{4} \frac{1}{z} \int \frac{\mathrm{d}k_h^-}{(2\pi)^n} \gamma^+ \quad k
\end{aligned}
\tag{12.39}
$$

Here we assume we work with an unpolarized situation, where there is a spin average on the quark; this gives a factor $\mathrm{Tr}_{\mathrm{Dirac}}/2$. There is another factor of $\frac{1}{2}$ that arises in the same way as for the pdf for a Dirac parton. The corresponding integrated fragmentation function is

$$
\begin{aligned}
d_{(0)\,h/j}(z) &= \frac{\mathrm{Tr}_{\mathrm{color}}}{N_{c,j}} \frac{\mathrm{Tr}_{\mathrm{Dirac}}}{4} \sum_X z^{n-3} \int \frac{\mathrm{d}x_h^-}{2\pi} e^{ik^+ x_h^-} \\
&\qquad \times \gamma^+ \langle 0 | \psi_j^{(0)}(x/2) | p, X, \mathrm{out} \rangle \langle p, X, \mathrm{out} | \bar{\psi}_j^{(0)}(-x/2) | 0 \rangle \\
&= \frac{\mathrm{Tr}_{\mathrm{color}}}{N_{c,j}} \frac{\mathrm{Tr}_{\mathrm{Dirac}}}{4} z^{n-3} \int \frac{\mathrm{d}k_h^-\, \mathrm{d}^{n-2}\boldsymbol{k}_{h\,\mathrm{T}}}{(2\pi)^n} \gamma^+ \quad k
\end{aligned}
\tag{12.40}
$$

12.4.5 Unpolarized Dirac antiquark

The same approach works for fragmentation functions in an antiquark. The result is that (12.40) can be used to define the fragmentation function of an antiquark, just with the positions of the ψ and $\bar{\psi}$ field exchanged, and the natural change in the flow of indices.

12.4.6 Renormalization

In a renormalizable theory, the integral over k^- and $\boldsymbol{k}_{\mathrm{T}}$ for an integrated fragmentation function has a UV divergence quite similar to that of a parton density. Renormalization works in the same way as for parton densities (Secs. 8.3 and 11.4). This leads to the statement of renormalization already given in (12.15).

12.4.7 Polarized Dirac quark

The hard scattering can generate a polarized quark, whose state is parameterized (Sec. 6.4.1) by a helicity λ and a transverse Bloch vector $\boldsymbol{s}_{\mathrm{T}}$. To deal with the most general case, we make the following replacement in the definition of the fragmentation function (integrated or unintegrated):

$$\frac{1}{4} \operatorname*{Tr}_{\mathrm{Dirac}} \gamma^+ \ldots \mapsto \frac{1}{4} \operatorname*{Tr}_{\mathrm{Dirac}} \gamma^+ (1 + \gamma_5 \lambda - \gamma_5 \boldsymbol{\gamma}_{\mathrm{T}} \cdot \boldsymbol{s}_{\mathrm{T}}) \ldots \qquad \text{(quark)}, \qquad (12.41\text{a})$$

$$\frac{1}{4} \operatorname*{Tr}_{\mathrm{Dirac}} \gamma^+ \ldots \mapsto \frac{1}{4} \operatorname*{Tr}_{\mathrm{Dirac}} \gamma^+ (1 - \gamma_5 \lambda - \gamma_5 \boldsymbol{\gamma}_{\mathrm{T}} \cdot \boldsymbol{s}_{\mathrm{T}}) \ldots \qquad \text{(antiquark)}, \qquad (12.41\text{b})$$

These projections are applied in the *hadron frame*. They arise from the wave functions used in light-front quantization, which correspond to those for massless Dirac particles. They are obtained from (A.27), which is surrounded by factors of γ^+ from the formula (6.64b) that gives the light-front annihilation operator. This reverses the sign of the helicity term relative to (A.27). Note also the reversal of the sign of the helicity terms between the quark and antiquark cases. The definitions of λ and $\boldsymbol{s}_{\mathrm{T}}$ are normalized to have a maximum value of unity (for a pure state).

The effects of polarization depend on the situation:

- For an integrated fragmentation function, the situation is like that for the pdfs. From a combination of parity invariance and conservation of angular momentum about the z axis, we find the following.
  - If the measured hadron is spinless, like a pion, or if its polarization is not detected, then there is no dependence on λ and $\boldsymbol{s}_{\mathrm{T}}$. Only the unpolarized fragmentation function is non-zero; our original definition suffices. This is the most common case.
  - If the measured hadron has spin $\frac{1}{2}$, then there are polarized fragmentation functions comparable to the Δf and $\delta_T f$ parton densities, with the analogous interpretations.
  - It is possible to generalize the definition of the fragmentation function to have two (or more) nearby measured hadrons instead of one. In dihadron fragmentation the

azimuthal distribution of the hadrons can be correlated with the transverse spin of the
quark, and an appropriate fragmentation function is defined (Collins, Heppelmann,
and Ladinsky, 1994), for which measurements can be found in Airapetian *et al.* (2008);
Vossen *et al.* (2009); Wollny (2009).

– For a spin-1 gluon, further possibilities arise which have not been explored in the
literature.

• For a k_T-dependent unintegrated fragmentation function, angular momentum can be
taken up by the azimuthal dependence of the measured hadron. The possibilities are
described by several fragmentation functions:

– The unpolarized fragmentation function defined above, which gives a uniform distri-
bution in the azimuthal angle of k_T or $p_{p T}$, i.e., this fragmentation function depends
only on the size of the transverse momentum.

– The Collins function. This is obtained from the $\gamma^+ \gamma_5 \boldsymbol{\gamma}_T \cdot \boldsymbol{s}_T$ part of the trace (Collins,
1993). It gives a characteristic $\sin \phi$ dependence, where ϕ is the azimuthal angle of the
hadron relative to the quark spin. See Boer (2008) for a review of recent theoretical
and experimental work.

– Other possibilities involving a detected hardron polarization. These have undergone
little investigation.

See Sec. 13.4.1 for more details.

12.4.8 Sum rules and symmetry properties

Momentum sum rule

In a fragmentation function, we have a state created by a light-front creation operator:
$a^\dagger_{j,k^+,k_T} |0\rangle$, and we project it onto a particular final state $|p, X, \text{ out}\rangle$. The total plus momen-
tum in the final state is k^+. We can measure the plus momentum in the final state by
integrating the fragmentation function over all p, with a weight p^+, and summing over all
hadron types. Dividing by k^+ gives the momentum sum-rule:

$$\sum_h \int_0^1 \mathrm{d}z \, z d_{(0)\, h/j}(z) = \sum_h \int_0^1 \mathrm{d}z \, z d_{h/j}(z) = 1. \qquad (12.42)$$

The derivation applies to the bare quantities. As with the sum rules for parton densities,
it implies that there is no UV divergence in the sum over h of the second moment, and
therefore that if we use a suitable renormalization scheme, like $\overline{\text{MS}}$, the sum rule applies
also to the renormalized fragmentation functions, as indicated above.

Flavor relations

There is one fragmentation function for each combination of hadron type and parton
type. In QCD, even with just pions, and light quarks and antiquarks and gluons, this
gives 21 fragmentation functions. But many of these can be related by applying isospin
transformations and charge conjugation transformations. This leaves just four independent
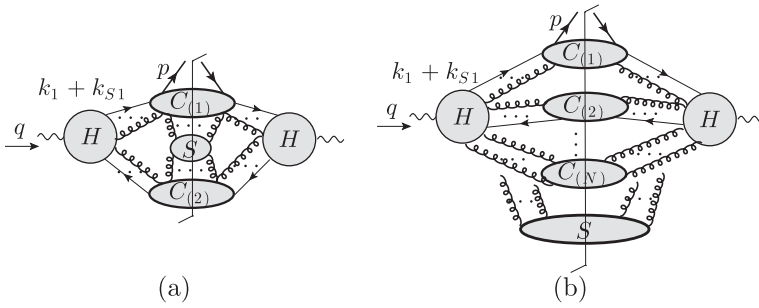
Fig. 12.4. Leading regions in gauge theory for one-hadron-inclusive cross section. The subgraphs H are the hard subgraphs, and there can be any number (greater than 2) of collinear subgraphs $C_{(1)}$, $C_{(2)}$, ..., of which two examples are shown. The soft subgraph may have any number of connected components, including zero. In (b), each gluon from the soft subgraph may connect to any collinear subgraph.

fragmentation functions

$$d_{\pi^+/u}(z) = d_{\pi^-/d}(z) = d_{\pi^-/\bar{u}}(z) = d_{\pi^+/\bar{d}}(z), \tag{12.43a}$$

$$d_{\pi^-/u}(z) = d_{\pi^+/d}(z) = d_{\pi^+/\bar{u}}(z) = d_{\pi^-/\bar{d}}(z), \tag{12.43b}$$

$$d_{\pi^+/s}(z) = d_{\pi^0/s}(z) = d_{\pi^-/s}(z) = d_{\pi^+/\bar{s}}(z) = d_{\pi^0/\bar{s}}(z) = d_{\pi^-/\bar{s}}(z), \tag{12.43c}$$

$$d_{\pi^+/g}(z) = d_{\pi^0/g}(z) = d_{\pi^-/g}(z). \tag{12.43d}$$

From these we obtain π^0 fragmentation functions of u and d quarks:

$$d_{\pi^0/u}(z) = d_{\pi^0/\bar{u}}(z) = d_{\pi^0/d}(z) = d_{\pi^0/\bar{d}}(z) = \frac{1}{2}[d_{\pi^+/u}(z) + d_{\pi^-/u}(z)]. \tag{12.43e}$$

by a Clebsch-Gordan decomposition of the final state. Only isospin $\frac{1}{2}$ and $\frac{3}{2}$ are possible for the X part of the state when the initiating parton has $I = \frac{1}{2}$ and the detected hadron has $I = 1$.

12.5 Leading regions and issues in a gauge theory

In a gauge theory, like QCD, the power-counting rules of Ch. 5 show that the general leading region (and its associated PSS) has the form specified by Fig. 12.4. Each electromagnetic vertex is part of a hard-scattering subgraph H, and out of each H exit two or more groups of lines of high energy and low virtuality. These groups each go into a collinear subgraph which crosses the final-state cut. To the collinear subgraphs may be connected a soft subgraph S (which consists of any number of connected components and can be absent).

We define the first collinear subgraph $C_{(1)}$ to be the one attached to the detected hadron. Consequently the direction for the corresponding collinear singularity of the region's PSS is fixed by p. The distinctness of the collinear configurations implies that the different collinear groups are treated as being at wide angle to each other. However, the angles of the other collinear groups are to be integrated over. When two or more of the directions get close, the
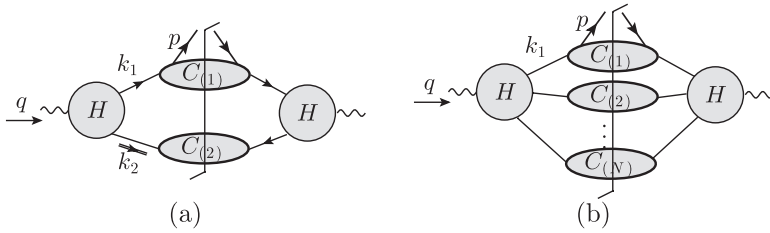
Fig. 12.5. Leading regions in *non*-gauge theory.

originally separate collinear configurations combine into a single collinear configuration, i.e., the corresponding jets merge into a single jet. In defining the contribution $C_R \Gamma$ for a region R with N collinear groups, there are subtractions for smaller regions, in particular for regions with fewer collinear groups. This results in a suppression of $C_R \Gamma$ where the angles of two or more collinear groups approach each other. Note that before subtractions there is a logarithmic enhancement after angular integration between a separated jet configuration and a merged jet.

The basic situation is more easily visualized by the leading regions in a model theory *without* gauge fields, in Fig. 12.5. Then there is no soft subgraph, and each collinear subgraph is initiated by a single parton, which can correspond to any of the fields in the theory. For a leading power, only one collinear line on each side of the final-state cut initiates each collinear subgraph, whose final state is essentially a jet.

To return to QCD, we have any number of extra gluons joining each collinear subgraph to the hard subgraphs, and we have a possible soft subgraph with gluonic couplings to any of the collinear subgraphs. Basically all these extra gluons have the polarization that we characterize as a Grammer-Yennie K gluon, as defined in Sec. 11.2.3.

Initially, each diagram like Fig. 12.4 codes a particular region of momentum space for some generic graph. According to the subtractive methods of Ch. 10, we reinterpret the diagram as an actual Feynman graph with integrals over *all* internal momenta, but with approximations applied that are appropriate for the region, and with subtractions to prevent double counting. Thus to leading power, the complete hadronic tensor $W^{\mu\nu}$ of (12.3) is a sum over all cases of Fig. 12.4.

12.5.1 Complication 1: super-leading regions

But one annoying extra possibility is generated by collinear groups that are purely gluon initiated. The amplitude between a photon and two gluons is prohibited by charge-conjugation invariance, so the smallest case is three collinear groups (Fig. 12.6). Just as we found with DIS in Secs. 11.2.3 and 11.3, there are graph-by-graph super-leading contributions, when all the external gluons of a collinear subgraph are K gluons. The Ward-identity arguments of Sec. 11.9 show that there is a cancellation after a sum over all graphs for the hard scattering. The result is that the gluons attaching to the hard subgraphs combine to give the operator defining the collinear factor, with its Wilson line.
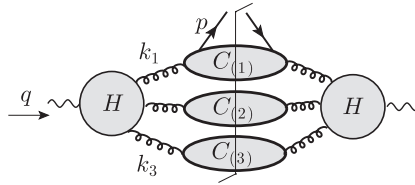
Fig. 12.6. A possible leading region in gauge theory, where all the jets are gluon initiated. Possible extra collinear gluons and a soft subgraph are not shown, for simplicity.
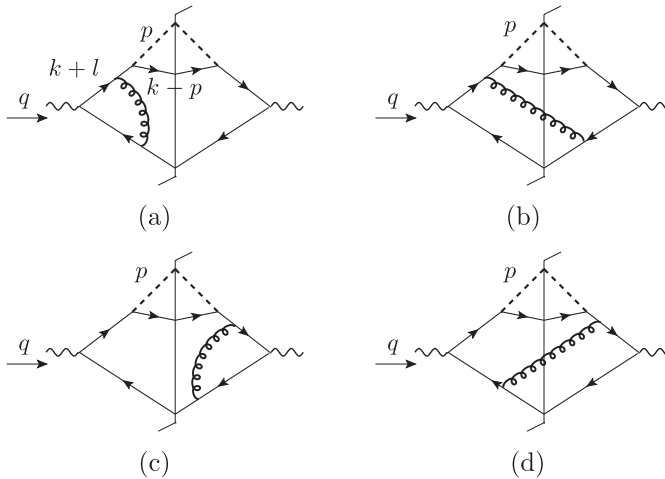

Fig. 12.7. To illustrate soft cancellation. The quarks and the pion (modeled by an elementary scalar field) form two collinear groups. The gluon is soft, and emitted off an internal line.

12.5.2 Complication 2: soft gluons and sum-over-cuts

Another complication is that to get the expected factorization theorem we need to show the soft factor cancels. The basic tool for getting the necessary cancellations is a sum-over-cuts. In the case of DIS, this was implemented in the conversion from a cut hadronic tensor $W^{\mu\nu}$ to the corresponding uncut quantity $T^{\mu\nu}$, in Sec. 11.2. But this argument is insufficient for our current process, because the final-state cut is restricted by being anchored at the detected hadron. This prevents the basic sum-over-cuts argument from combining some of cut graphs relevant to the cancellation of soft gluon effects, and we will need a more powerful argument to be given later.

As a simple example, consider the graphs in Figs. 12.7 and 12.8. We have chosen a model in which the pion is replaced by an elementary scalar field with a Yukawa coupling to the quarks. The pion analog may or may not be color singlet. We choose kinematics in which there is a quark and an antiquark jet, with the quark collinear to the pion, and then we add a soft gluon.

(a)   (b)

(c)   (d)

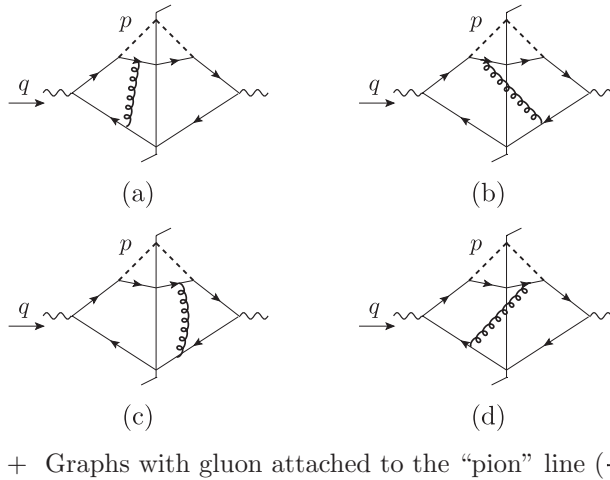+ Graphs with gluon attached to the "pion" line (------).

Fig. 12.8. The same as Fig. 12.7, but with soft gluon emission off the external quark in the upper jet.

First consider graphs where the gluon is emitted off the internal quark line (Fig. 12.7). Graphs (a) and (b) are related by moving the final-state cut, as are graphs (c) and (d). But cancellation within each pair of graphs is not sufficient to get a soft gluon cancellation; see problem 12.4 and Sec. 12.5.3. Graphs (c) and (d) are needed in the cancellation, but are not related to (a) and (b) by moving the final-state cut. Moreover, the cancellation will need, among others, a term that behaves as if the cut were moved to the leftmost quark-antiquark pair in graph (a); but this cut does not keep the pion analog in the final state.

To demonstrate cancellation of the soft subgraphs, we first factorize the soft subgraph, just as for the Sudakov form factor in Ch. 10. In our example this requires us to sum all ways of attaching the soft gluon to the lines in the collinear graph, and thus to include the diagrams with external-line emission of the soft gluon (Fig. 12.8). After applying the soft approximation and Ward identities, we get a factorized result:

$$\int \frac{\mathrm{d}^4 q_S}{(2\pi)^4} \quad \text{} \quad \times \quad \sum_{\text{cuts}} \text{} \tag{12.44}$$

Here the first factor is just as in a non-gauge theory, and is a product of two collinear factors. The soft gluon is in second factor, where it is attached to eikonalized quark lines (i.e., Wilson lines). The sum-over-cuts argument applies to the soft factor:

$$\sum_{\text{cuts}} \text{} = \text{} + \text{} \tag{12.45}$$

and as with the corresponding argument for the total cross section in Sec. 4.4, we will see in Sec. 12.7 that this implies that the integration is not trapped in the soft region.

12.5.3 KLN theorem is not sufficient

The above summary indicates that the cancellation of soft gluons is obtained somewhat indirectly: first the soft part is factorized, and then the sum-over-cuts argument is applied. Now the soft-gluon issue is a generalization of the IR-divergence problem in QED. It is therefore tempting to suppose that a more direct proof of cancellation can be done by appealing to the theorem of Kinoshita (1962) and Lee and Nauenberg (1964) (KLN theorem). This theorem is well known in applications to QED, and it also applies to the e^+e^- total cross section discussed in Sec. 4.1. The KLN theorem (together with minor generalizations) applies when the canceling terms are related by a sum-over-cuts of individual graphs.

With a massless gluon, the KLN theorem does indeed show that the actual IR divergences cancel. These arise from where the gluon momentum goes to zero, and therefore only from graphs like Fig. 12.8, where the IR gluons are emitted from external lines. In this case the sum-over-cuts argument succeeds. But for merely soft gluons we use a much broader range of gluon momenta: any that are much less than Q and central in rapidity. Then internal line emission, Fig. 12.7, is also important.

To see this explicitly, we apply power-counting from Ch. 5 to the loop momenta defined in Fig. 12.7(a). We characterize the relative transverse momentum of the upper collinear lines by λ, so that the pion-quark invariant mass is of order λ^2. We let the size of the soft momentum l be of order λ_S in all components. The size of the denominator of an internal line carrying soft and collinear momenta is then

$$(k + l)^2 - m_q^2 = O(\lambda^2) + O(Q\lambda_S). \tag{12.46}$$

For lines next to an external line attachment, the λ^2 term is missing:

$$(k - p + l)^2 - m_q^2 = O(Q\lambda_S), \tag{12.47}$$

because the momentum $k - p$ is exactly on-shell.

IR gluon: $\lambda_S \ll \lambda^2/Q$

When λ_S is sufficiently small, much less than λ^2/Q, graphs with emission from external lines give logarithmic power-counting, from the external line factors (12.47) and the gluon line. This gives an IR divergence in the graphs of Fig. 12.8, if the gluon is massless. Internal line emission, Fig. 12.7, is suppressed because a denominator of order $Q\lambda_S$ is replaced by a much larger denominator of order λ^2; see (12.46).

Hence in this region only external line emission is important, and the KLN theorem applies.

Harder gluon: $\lambda_S \gg \lambda^2/Q$

When the contrary situation holds, i.e., $\lambda_S \gg \lambda^2/Q$, internal-line emission, Fig. 12.7, dominates. In this case those collinear denominators that carry soft momentum are of order $\lambda_S Q$; collinear denominators without a soft momentum have the much smaller value λ^2.

Relative to a graph without the soft gluon, internal line emission has two collinear denominators of order $\lambda_S Q$, and we get logarithmic power-counting, and hence a contribution at leading power. But for external line emission, a second collinear denominator λ^2 is replaced by an extra larger $\lambda_S Q$ denominator, which is much larger and therefore leads to a suppression.

Borderline: $\lambda_S \sim \lambda^2/Q$

In the intermediate range of gluon momentum both internal and external emission are equally important.

Combination is simple

The Ward-identity argument for soft gluons combines all the above contributions and applies independently of the relative size of λ_S and λ. We get a coherent sum over gluon emission from the whole jet, and the result is as if the gluon were emitted from a single quark, as in the right-hand factor in (12.44). In this factor we have uniform power-counting independently of the relative size of λ_S and λ.

12.6 Which gauge to use in a proof?

Our characterization of leading regions was appropriate to Feynman gauge. But, as we saw in Sec. 5.5, the situation is gauge dependent.

The most notable effect is in the axial gauge, $n \cdot A = 0$, for which numerator of the gluon propagator is (5.40). We choose the gauge-fixing vector n proportional to q, i.e., to be at rest in the overall center-of-mass frame (Collins and Sterman, 1981). Then the enhancement of gluons connecting a collinear subgraph to a hard subgraph is removed. Regions with extra gluons connecting collinear to hard subgraphs, as in Fig. 12.4, are now power-suppressed. Regions with gluon-generated jets, Fig. 12.6, are merely leading instead of super-leading. To see this, we observe that in the rest frame of a collinear momentum, the gauge-fixing vector n is approximately a light-like vector w_2, and that the same light-like vector can be used in the Grammer-Yennie K term, (11.6), when the gluon attaches to the hard scattering. The K term then gives zero, because the $w_2^{\nu_j}$ factor in (11.6) contracts with a gluon propagator which is being treated as if it were in $w_2 \cdot A = 0$ gauge.

More formally, consider a collinear subgraph for a region R, and let w_1 be the light-like vector for the subgraph's momenta on the PSS for the region. We let w_2 be the conjugate light-like vector used in the Grammer-Yennie decomposition (11.6) for the attachment of a collinear gluon to the hard subgraph. Define light-front coordinates such that $w_1^\mu = \delta_+^\mu$ and $w_2^\mu = \delta_-^\mu$. Then for a collinear momentum k, its contraction with the gauge-fixing vector is $k \cdot n \simeq k^+ n^- = k \cdot w_2 n \cdot w_1$. By scaling n we can set $n^- = 1$, and therefore to leading power, $k \cdot n \simeq k \cdot w_2$, i.e., we can replace n by w_2 on collinear gluons. The w_2 factor in the K-gluon definition gives zero when contracted into the approximated propagator.

In the $n \cdot A = 0$ gauge, a Wilson line in direction n is simply unity. So if this Wilson line were used in the definition of a fragmentation function or parton density, the Wilson
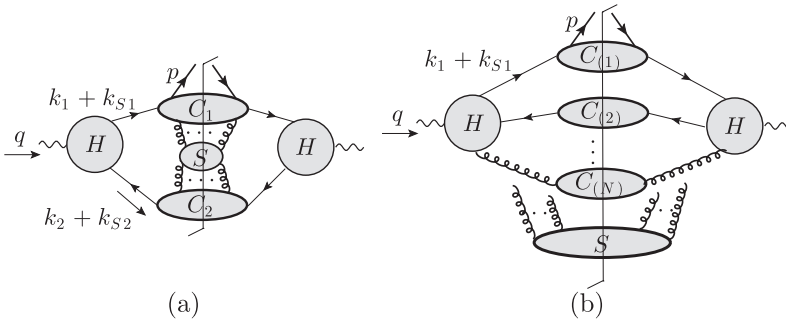
Fig. 12.9. Leading regions in gauge theory for one-hadron-inclusive cross section, now in $n \cdot A = 0$ gauge for case of (a) two and (b) more collinear groups.

line could be ignored in the $n \cdot A = 0$ gauge. Therefore such a definition has the same form as in a non-gauge theory.

But we still have a soft subgraph, unlike the case in a non-gauge theory. The resulting leading regions are illustrated in Fig. 12.9. A further advantage of an axial gauge is that Ward identities in a non-abelian theory are simple: they are essentially the same as in an abelian theory, without the terms involving Faddeev-Popov ghosts.

On all of these points, the axial gauge is superior to the Feynman gauge. However, one issue reverses the situation. This is that the necessary contour deformation out of the Glauber region is often obstructed in axial gauge.

Recall that the Glauber region is where the longitudinal momentum of a gluon is much less than its transverse momentum. The Ward-identity method to extract soft gluons from a collinear subgraph uses an approximation of the Grammer-Yennie type. But the approximation fails in the Glauber region. In Feynman gauge, the normal causal structure of Feynman denominators allows a deformation out of the Glauber region; the argument in Sec. 5.5.10 applies to the process we are considering, since all the partons are outgoing from a single interaction point.

But in the axial gauge there are unphysical singularities $1/k \cdot n$ in the gluon propagator, and these have the potential to obstruct the contour deformation.

Consider, for example, the vertex graph Fig. 5.21 for the Sudakov form factor, which also appears as a subgraph in hadron production in $e^+ e^-$ annihilation. In Feynman gauge, we get out of the Glauber regions the gluon momentum k, by using any deformation of the form

$$k^+ \mapsto k^+ + iC, \quad k^- \mapsto k^- - iD, \tag{12.48}$$

where both C and D are non-negative, and at least one is positive. In an axial gauge, we have $1/k \cdot n$ singularities, which are principal value, and therefore prevent any deformation on $k \cdot n = k^+ n^- + k^- n^+$. The non-deformation can be satisfied by setting $C/D = n^+/n^-$, which requires that n be time-like. If we use the center-of-mass frame, and choose $n \propto q$, then we need $C = D$, so that on the deformed contour the imaginary parts of k obey $\Im k^0 = 0$ and $\Im k^3 > 0$. The gauge condition in use here is $A^0 = 0$.

More generally, as in Fig. 12.9, we can have extra collinear subgraphs, and multiple soft gluon loops. Consider a soft momentum k routed out through one collinear subgraph and back through another. Let the light-like directions for the collinear subgraphs be w_1 and w_2. Then in the collinear subgraphs we have propagators like

$$\frac{1}{(k_1 - k)^2 - m^2 + i0} = \frac{1}{-2k \cdot w_1 \times \text{positive} + \cdots + i0}, \tag{12.49a}$$

$$\frac{1}{(k_2 + k)^2 - m^2 + i0} = \frac{1}{2k \cdot w_2 \times \text{positive} + \cdots + i0}. \tag{12.49b}$$

We avoid these singularities by deforming with imaginary parts such that $\Im k \cdot w_1 < 0$ and $\Im k \cdot w_2 > 0$. In addition, we require $\Im k^0 = 0$ to avoid the axial gauge singularities, and then $\Im k^3 > 0$. The Coulomb gauge, (10.156), is also compatible with such a deformation: its unphysical singularities are not operative in the Glauber region, where $k^\pm \ll k_T$.

While this all appears to work for inclusive processes in $e^+ e^-$ annihilation, it does not help in other processes we consider. For example, for SIDIS (Sec. 12.14) the avoidance of poles in collinear propagators will restrict the deformations incompatibly with the axial gauge. In an equivalent of (12.48), we will need D to be zero: k^+, but not k^-, is not to be deformed. In the Drell-Yan and other reactions in hadron-hadron collisions (Ch. 14) we will need more elaborate arguments. Different parts of the proof will need different deformations, some on plus-components and some on minus-components of loop momenta; such different deformations are prevented by an axial gauge.

The offending singularities for the axial gauge are in a gauge-dependent part of the propagator, so their effects should cancel in the final result for a gauge-invariant amplitude. What is not clear is how to make this demonstration while at the same time preserving the rest of a factorization proof, and to the best of my knowledge has not been done.

So we conclude that for fully general and reliable proofs one should use Feynman gauge. Even if we can avoid the problems of axial (or Coulomb) gauge for a subset of processes, the methods of proof do not extend to other important cases.

In summary, here is a list of possible approaches, including some not mentioned above:

- Time-like axial gauge. This gave the first good approximation to a proof (Collins and Sterman, 1981) of factorization in $e^+ e^-$ annihilation. The leading regions and the Ward identities are relatively simple, but the Glauber region cannot be handled for more general processes.
- Coulomb gauge. The extra singularities in the gluon propagator are $1/\mathbf{k}^2$ instead of $1/n \cdot k$, which improves the Glauber problem, but not sufficiently for a general process. In addition, there are complications in setting up the Coulomb gauge in a non-abelian theory.
- A non-covariant generalization of the Feynman-type gauges proposed by Sterman (1978, Sec. V). The extra gluon connections between collinear and hard subgraphs are suppressed, but the unphysical singularities are now off the real axis, so at a first approximation this allows a contour deformation out of the Glauber region. But the singularities

are such as not to allow all the needed contour deformations, and definitely not in semi-inclusive DIS.

- Light-cone gauge, where n is light-like. This suppresses extra connections from a collinear to a hard subgraph, but only for one collinear direction. So this gauge is of use in ordinary fully inclusive DIS, where the only direction of collinearity is that of the target hadron. But the light-cone gauge does not help when there are multiple directions of collinearity. This gauge also has problems with rapidity divergences, which fail to cancel in transverse-momentum-dependent parton densities and fragmentation functions (Ch. 13).
- Covariant gauge.
- A more recent and very popular approach is that of soft-collinear effective theory (Fleming, 2009). See Sec. 15.9 below for my comments.

12.7 Unitarity sum over jets/sum over cuts

Before we go to the proof of factorization for the process (12.1), it is useful to examine in its simplest setting a method that is repeatedly used in proofs of factorization. The method is that of summing over cuts of a region subgraph (for a collinear or soft region) when there are no detected final-state particles. The result is that momenta in the region subgraph are not trapped in regions of low virtuality after the sum-over-cuts, whereas momentum integrations are trapped for individual cut diagrams.

In this section, we examine the simplest case, which is for the collinear subgraphs $C_{(2)}, \ldots, C_{(N)}$ in the leading regions, Fig. 12.5, for a non-gauge theory. Once we have proved the momentum integrals are not trapped in these subgraphs, we can absorb these subgraphs in the hard subgraph, so that the effective leading regions are those in Fig. 12.2. It has a single collinear subgraph, $C_{(1)}$, the one containing the detected hadron. Precisely because the cut of $C_{(1)}$ is anchored to include the detected hadron, the sum-over-cuts argument fails for this one subgraph.

We combine as a group the sum of region graphs that are related by moving the final-state cut to cross different parts of the collinear subgraphs in Fig. 12.5. The cuts can be applied independently to each collinear subgraph $C_{(\alpha)}$. We use a version of the Cutkosky (1960) rules to relate the sum-over-cuts of $C_{(\alpha)}$ to corresponding uncut amplitudes:

 (12.50)

In the overall center-of-mass frame, we write the momenta of the subgraph's lines as $l_{\alpha i} = (E_{\alpha i}, \boldsymbol{l}_{\alpha i})$, with the index i labeling the lines.

First we convert the Feynman graphs to time-ordered graphs (exactly as for x^+ perturbation theory in Sec. 7.2). The integrand in each term in time-ordered perturbation theory corresponds to a sequence of intermediate states with energy denominators:

$$I(b) = \prod_{a=1}^{b-1} \left[\frac{i}{E - E_a + i\epsilon} (ig) \right] 2\pi \delta(E - E_b) \prod_{c=b+1}^{n} \left[(-ig) \frac{-i}{E - E_c - i\epsilon} \right]. \quad (12.51)$$

Here there is a set of n intermediate states, with state number b being cut. The part to the right of the final-state cut is a complex-conjugated amplitude. The energy of state a is E_a when all its lines are on-shell, and the external energy entering from the hard scattering is $E = k_\alpha^0$. Multiplying the above formula is a common factor that depends only on the 3-momenta of the lines, and is independent of the position of the cut.

It is easily proved that the sum-over-cuts gives

$$\sum_{b=1}^{n} I(b) = (ig)^{n-1} \prod_{a=1}^{n} \frac{i}{E - E_a + i\epsilon} + (-ig)^{n-1} \prod_{c=1}^{n} \frac{-i}{E - E_c - i\epsilon}. \qquad (12.52)$$

The proof is made by using the identity

$$2\pi\delta(E - E_b) = \frac{i}{E - E_b + i\epsilon} + \frac{-i}{E - E_b - i\epsilon}, \qquad (12.53)$$

and showing that in the sum over b, there is a cancellation of all the resulting terms except for the two on the r.h.s. of (12.52). Converting back to Feynman perturbation theory gives (12.50).

We now use the same idea as with the e^+e^- total cross section in Sec. 4.4. This uses the property that all the poles in E are on one side of the real axis in each uncut collinear subgraph on the r.h.s. of (12.52). We arrange to deform the integration over E, so that the contour no longer goes close to the poles. The propagators are now far off-shell, and we can treat the collinear graphs $C_{(2)}$ to $C_{(N)}$ as part of the hard scattering. *Effectively* the leading regions are of the form of Fig. 12.2, where the only collinear subgraph is the one containing the detected hadron.

To implement the contour deformation, we use the averaged hadronic tensor defined in Sec. 12.1.2. This enables us to route the total momentum k_α of each collinear subgraph through the hard scattering and out at the virtual photon vertex. The averaging function is then $f(\sum_{\alpha=1}^{N} k_\alpha)$, and we do not have to route each k_α back through another collinear subgraph. The averaging function is slowly varying as a function of Q, and the hard scattering involves dominantly highly virtual momenta, so neither obstructs the contour deformation.

In reality, the hard subgraph can have collinear and soft singularities, but these are suppressed by subtractions. When we deform the E integration for a collinear subgraph, singularities in the hard scattering must be crossed. But the resulting contributions are power-suppressed because of the subtractions, and we therefore ignore them.

12.8 Factorization for $e^+e^- \to h(p) + X$ in gauge theory

The proof of factorization in Feynman gauge uses the methods of Ch. 10 supplemented by the non-abelian Ward-identity results for K gluons in QCD given in Sec. 11.9. Given these techniques and the associated graphical notation, the proof can be given quite quickly. Any issues about the accuracy of the proof really concern the earlier work.
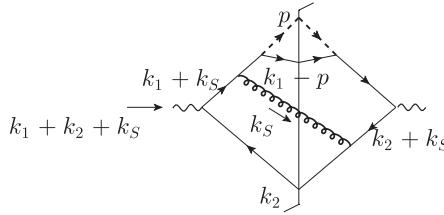
Fig. 12.10. Momentum routing for Fig. 12.7. The gluon is treated as soft, and the quarks as collinear in one of two directions.

A new feature relative to DIS is that the cancellation of the soft subgraphs occurs at a late stage. Therefore much of the proof will apply equally to situations (Ch. 13) where the soft cancellation does not happen because of more stringent conditions on the final state.

The proof starts from the leading regions symbolized diagrammatically in Fig. 12.4.

12.8.1 Definition of approximators

We now apply the principles for making the approximator for a region that we formulated in Secs. 10.4 and 10.6.

Momentum routing

Soft loop momenta flow between the soft subgraph into collinear subgraphs. We define them to flow outwards to the electromagnetic vertex. As illustrated in Fig. 12.10, to avoid routing soft momenta back through the final state of a collinear graph, we route them out of the electromagnetic vertex. This takes advantage of our definition (12.11) of averaging the hadronic tensor with a test function. We label the collinear subgraphs by α: $1 \leq \alpha \leq N$; we let the momenta of the lines from H to C_α be $k_{\alpha i}$.

Light-like auxiliary vectors w_α and $\tilde{w}_\alpha$ for collinear subgraph $C_{(\alpha)}$

Auxiliary vectors w_α and $\tilde{w}_\alpha$ are defined as follows:

- For each collinear subgraph $C_{(\alpha)}$, we define a characteristic momentum p_α. For the collinear subgraph $C_{(1)}$ that contains the detected hadron, we use $p_1 = p$, the momentum of the detected hadron. For the other collinear subgraphs, p_α is the total final-state momentum of the collinear subgraph, i.e., $p_\alpha = \sum_i k_{\alpha i}$.
- For each $C_{(\alpha)}$, the corresponding light-like direction is

$$w_\alpha^\mu = \frac{Q}{\sqrt{2} p_\alpha \cdot q} \left[\frac{p_\alpha^\mu - q^\mu \, p_\alpha \cdot q / q^2}{\sqrt{1 - p_\alpha^2 Q^2 / (p_\alpha \cdot q)^2}} + \frac{q^\mu \, p_\alpha \cdot q}{q^2} \right]. \qquad (12.54)$$

In the center-of-mass frame, the direction of the 3-vector part is that of p_α.

- The conjugate auxiliary vector is defined by

$$\tilde{w}_\alpha^\mu = \frac{q^\mu}{w_\alpha \cdot q} - \frac{w_\alpha^\mu q^2}{2(w_\alpha \cdot q)^2}. \qquad (12.55)$$

- For each collinear group, the auxiliary vectors can be regarded as defining light-front coordinates in which $(w_\alpha^\mu)_{\text{frame } \alpha} = \delta_+^\mu$ and $(\tilde{w}_\alpha^\mu)_{\text{frame } \alpha} = \delta_-^\mu$. Note carefully that this is a different frame for each collinear group.
- For use in the soft approximation, we generalize the definitions (10.15b) of n_1 and n_2. For each α, we choose a rapidity parameter y_α, and define a space-like vector by

$$n_\alpha^\mu = w_\alpha^\mu - e^{-2y_\alpha} \tilde{w}_\alpha^\mu. \tag{12.56}$$

As in Sec. 10.4.2, the letter w denotes a light-like vector and n denotes a non-light-like vector.

Approximators

We split the gluons connecting different subgraphs into K and G terms, as in Sec. 11.2.3:

- For a K gluon attaching collinear subgraph α to a hard subgraph H, we copy (11.32).

$$H^\mu(k_{\alpha i}) \, C_{(\alpha),\mu}(k_{\alpha i}) = H^\mu(\hat{k}_{\alpha i}) \frac{\hat{k}_{\alpha i, \mu} \tilde{w}_\alpha^\nu}{k_{\alpha i} \cdot \tilde{w}_\alpha + i0} \, C_{(\alpha),\nu}(k_{\alpha i}), \tag{12.57a}$$

where

$$\hat{k}_{\alpha i}^\mu = \frac{w_\alpha^\mu \, k_{\alpha i} \cdot \tilde{w}_\alpha}{w_\alpha \cdot \tilde{w}_\alpha}. \tag{12.57b}$$

This projects the gluon's momentum onto direction w_α.
- For G gluons and quarks, we project the momentum by (12.57b).
- For a quark exiting the hard scattering to collinear subgraph α, we project its Dirac spinor onto a massless on-shell wave-function multiplying H by inserting a factor $\gamma^- \gamma^+/2$. This is made relative to light-front coordinates defined by w_α and $\tilde{w}_\alpha$. In covariant form, the projector is $\psi_\alpha \bar{\psi}_\alpha/(2w_\alpha \cdot \tilde{w}_\alpha)$.
- For an *anti*quark exiting the hard scattering, we use the projector $\bar{\psi}_\alpha \psi_\alpha/(2w_\alpha \cdot \tilde{w}_\alpha)$.
- At the coupling of a K gluon of S to collinear subgraph $C_{(\alpha)}$, we denote the line's momentum (out of $C_{(\alpha)}$) by $k_{S\alpha i}$, and define the soft approximant by

$$C_{(\alpha)}^\mu(k_{S\alpha i}) \, S_\mu(k_{S\alpha i}) = C_{(\alpha)}^\mu(\hat{k}_{S\alpha i}) \frac{\hat{k}_{S\alpha i, \mu} n_\alpha^\nu}{k_{S\alpha i} \cdot n_\alpha + i0} \, S_\nu(k_{S\alpha i}), \tag{12.58a}$$

where

$$\hat{k}_{S\alpha i}^\mu = \frac{\tilde{w}_\alpha^\mu \, k_{S\alpha i} \cdot n_\alpha}{\tilde{w}_\alpha \cdot n_\alpha}. \tag{12.58b}$$

This projects the soft momentum onto our defined conjugate direction for $C_{(\alpha)}$, and uses the non-light-like vector n_α to cut off the rapidity divergence that would otherwise occur at $k_{S\alpha i} \cdot w_\alpha = 0$.
- The approximated momenta are also used in the test function $f(q) = f(p + p_X)$ in (12.11). Thus the approximant changes $f(p + p_X)$ to $f(\sum_\alpha \hat{k}_\alpha)$, where $\hat{k}_\alpha$ is the total approximated momentum for collinear subgraph $C_{(\alpha)}$.

- Finally we redefine the hard-scattering factor by an extra factor:

$$H = \text{basic definition of } H \times \prod_{\alpha=2}^{N} \left(\frac{|\hat{\boldsymbol{k}}_\alpha|}{|\boldsymbol{k}_\alpha|} \right)^{n-2}. \tag{12.59}$$

Here $\boldsymbol{k}_\alpha$ is the total final-state momentum of collinear subgraph $C_{(\alpha)}$, and n is the space-time dimension.

At this point (12.59) is a totally unobvious redefinition. Note that, in the collinear limit, $\hat{\boldsymbol{k}}_\alpha \to \boldsymbol{k}_\alpha$, and the extra factor goes to unity. Hence the redefinition is one that is allowed; it is a change of factorization scheme. Appropriate versions of the redefinition will also appear, applied to smaller hard subgraphs, in the double-counting subtractions defining the region terms $C_R\Gamma$. The result is that the redefinition does affect the correctness of the factorization formula, but only the precise definition of the factors. Notice also that the redefinition involves only collinear but not soft momenta.

The rationale for the redefinition will appear in Sec. 12.8.5, where to get the most desirable form of factorization we will change the variables from k_α to $\hat{k}_\alpha$. The redefinition factor will cancel a part of the Jacobian for the change of variable. We will see that we only apply the redefinition to collinear subgraphs without an observed hadron, i.e., the case $\alpha = 1$ is omitted from the product in (12.59).

For the Sudakov form factor, we also rescaled the external momenta of H; see p. 329. We do not need to do this at this point in our case.

With these definitions, the approximated hard subgraph does not depend on the soft momenta, because a soft momentum in collinear subgraph α is approximated to be in direction $\tilde{w}_\alpha$. This gives a zero contribution in the projection (12.57b) onto an approximated momentum in H, because $\tilde{w}$ is light-like.

12.8.2 Extraction of collinear gluons from hard subgraph

We first extract the collinear gluons from the hard subgraphs.

The necessary result was given in Sec. 11.9.5, and stated graphically for the case of two collinear groups in Fig. 11.15. We apply this result on both sides of the final-state cut in Fig. 12.4, to obtain Fig. 12.11.

For example, suppose collinear subgraph $C_{(1)}$ has a quark entering it from the hard subgraph. When the accompanying K gluons are extracted from H, they couple to a Wilson line at the end of the quark line. On the left side of the final-state cut, the color matrices in the Wilson line are those appropriate to make a gauge-invariant operator with the $\bar{\psi}$ field that creates the quark entering $C_{(1)}$. The Wilson line extends out to infinity in the direction $\tilde{w}_1$. It represents a source of the opposite color to the parton initiating the collinear subgraph. Thus the Wilson line is an approximation to the rest of the event, seen as recoiling against collinear system $C_{(1)}$. In the mathematics, we get the Wilson line from graphs *omitted* from H because of the irreducibility requirements.

For a collinear subgraph initiated by an antiquark or a G gluon, the Wilson line has the corresponding color representation, and similarly on the right of the cut.
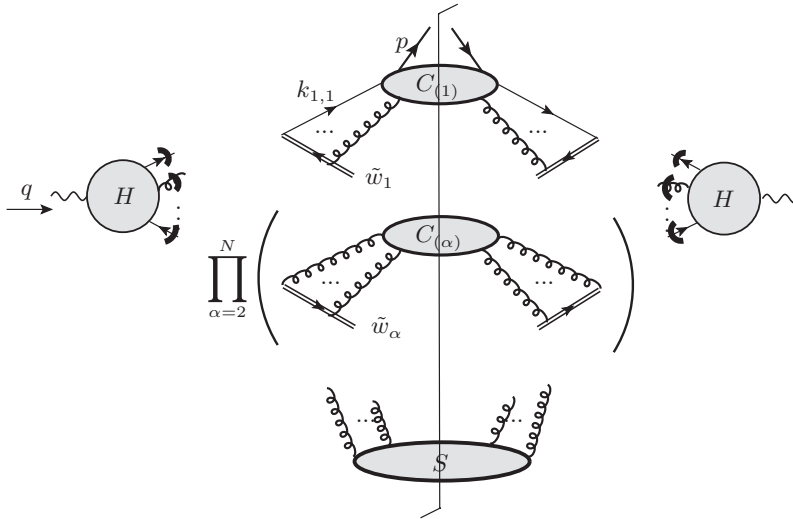
Fig. 12.11. Result of extraction of collinear K gluons from hard subgraphs in Fig. 12.4. There are Wilson lines for each subgraph in the directions shown. The soft subgraph S still couples to the collinear subgraphs. The little thick arcs on the hard subgraphs indicate on-shell partonic lines.

In accordance with our definitions, soft subtractions are applied in each collinear subgraph, and these remove rapidity divergences.

12.8.3 Factorization of soft subgraph

Similarly, we apply the Ward-identity argument to the connections of the soft subgraph to each collinear subgraph, to obtain Fig. 12.12.

Now in the extraction of collinear K gluons from a hard subgraph H, the external lines of H are on-shell. So the Wilson lines in Fig. 12.11 arose from the lack of collinear-reducible graphs in H. But for soft K gluons attaching to C_α, the irreducibility only concerns the K gluons themselves. As we saw in Sec. 11.9.5, these by themselves give no contribution; from the terms "missing" in the Ward identity due to irreducibility requirement we obtain commutator terms that are themselves of the K-gluon form. The on-shell external lines of $C_{(\alpha)}$ in the final state give no contribution to the Ward identity.

On each side of the final-state cut, each $C_{(\alpha)}$ has an external off-shell quark (or G gluon), with a Wilson line to make a gauge-invariant operator. But graphs are missing where external soft gluons directly couple to the Wilson line, since these did not come out of the argument that derived the Wilson lines. However, an approximated soft gluon gives zero when it attaches to the Wilson line, because the vertex for the Wilson line is proportional to $\tilde{w}_\alpha$. The K gluon specified in (12.58) multiplies this by $\hat{k}_{S\alpha i}$, and gives zero since $\hat{k}_{S\alpha i}$ is in the light-like direction $\tilde{w}_\alpha$.
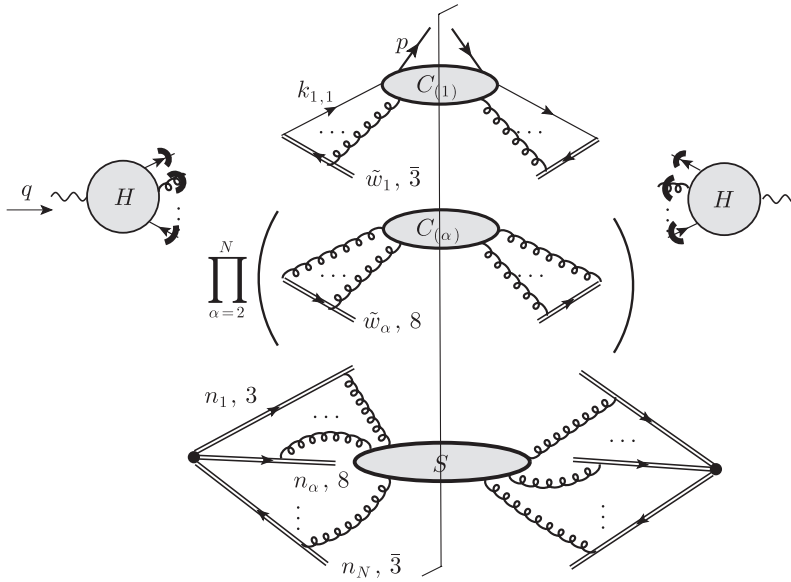
Fig. 12.12. Result of extraction of soft K gluons from collinear subgraphs in Fig. 12.11. The soft factor has a Wilson line for each external parton of the hard scattering, with the appropriate color charge, e.g., ("3", "8"). There is a non-trivial flow of color indices between the hard subgraph, the soft subgraph, and the collinear subgraphs; see Fig. 12.13 below.

So we can add to Fig. 12.11 all graphs where the soft gluons attach to the Wilson lines of $C_{(\alpha)}$. After applying the usual Ward-identity argument, we find that the soft gluons are moved to Wilson-line factors external to $C_{(\alpha)}$, as in Fig. 12.12.

12.8.4 Color flow

The Wilson lines are matrices in color space, and their color representation and color flow need attention. Each Wilson line of S has the color representation corresponding to the color charge of the outgoing parton initiating the associated jet.

The Wilson line for the gluons attaching S to $C_{(\alpha)}$ interposes itself between H and $C_{(\alpha)}$, as indicated in Fig. 12.13. We make a concrete illustration from the particular graph given in Fig. 12.14(a), which shows an extract from a particular diagram for the process we are analyzing. Diagram (b) shows one of the unapproximated graphs that are combined to give diagram (a) (after the use of approximators and Ward identities). Corresponding to diagram (a) is the formula

$$C_{(1)}(k_{1,1}, k_{1,2})_\mu \frac{i}{k_{1,2} \cdot \tilde{w}_1 + i0} (ig\tilde{w}_1^\mu t_\alpha)(-ign_1^\nu t_\beta) S(k_S)_\nu \frac{i}{k_S \cdot n_1 + i0} H(\tilde{w} \cdot (k_1 + k_2)).$$

$$(12.60)$$
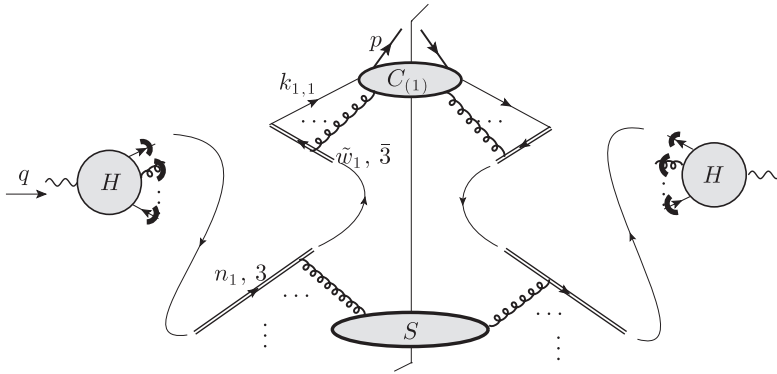
Fig. 12.13. Color flow between the hard subgraph, the soft subgraph S, and the collinear subgraphs. The vertical dots near S indicate that it has multiple Wilson lines, one on each side of the final-state cut for each $C_{(\alpha)}$.
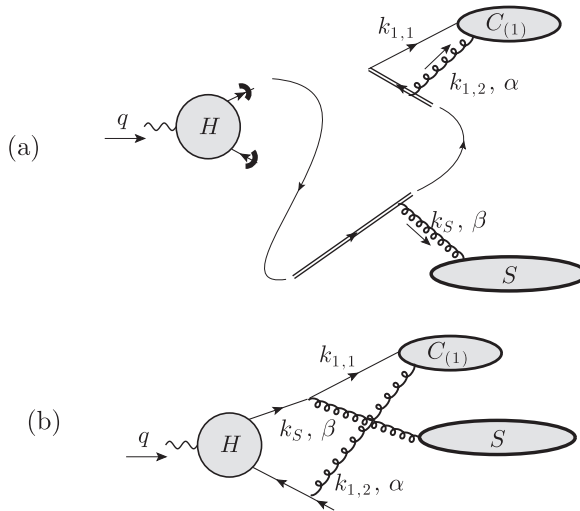
Fig. 12.14. (a) Specific example of Fig. 12.13. Each gluon is labeled with its momentum and color index. (b) A graph that, after approximants and Ward identities are applied, would contribute to (a).

The color charge (quark or antiquark) on a Wilson line is coded both in the ordering of the color matrices and in the sign of the vertices.

Now that all soft gluon lines have been extracted from the collinear subgraphs $C_{(\alpha)}$, each $C_{(\alpha)}$ becomes diagonal in color. This implies that we can rearrange the color flow as in Fig. 12.15. After rearrangement, there is an average over the color of each $C_{(\alpha)}$, i.e., a trace over colors divided by $N_{c\alpha}$, the number of colors for the parton initiating $C_{(\alpha)}$. That is, $N_{c\alpha}$ is 3 for the case of a quark or antiquark, but 8 for a gluon.
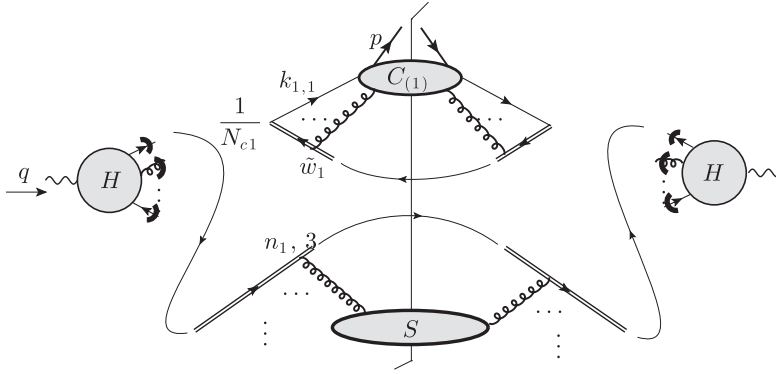
Fig. 12.15. Color flow of Fig. 12.13 after use of color-singlet property of C_1, with N_{c1} being the number of colors for the primary parton initiating C_1, which is a quark in the case shown, with $N_{c1} = 3$.

Then the color flow for the Wilson lines of S is direct from a Wilson line on the left of the cut to the Wilson line on the right; the collinear subgraphs are completely factored out. *But the color flow remains entangled with the color structure of the hard scattering.*

12.8.5 Factorization

We now have a factorized form for the hadronic tensor averaged with a function $f(q)$:

$$
W^{\mu\nu}([f], p) = \sum_{N \geq 2} \prod_{\alpha=1}^{N} \left[\sum_{j_\alpha} \int \frac{\mathrm{d}^n k_\alpha}{(2\pi)^n} C_{(\alpha), j_\alpha}(k_\alpha) \right] \int \frac{\mathrm{d}^n k_S}{(2\pi)^n} S_{j_1, \ldots j_N}(k_S)
$$

$$
\times H_{j_1, \ldots j_\alpha}(\hat{k}_1, \ldots, \hat{k}_N) \, f(\hat{k}_1 + \ldots + \hat{k}_N) \prod_{\alpha=2}^{N} \left(\frac{|\hat{\boldsymbol{k}}_\alpha|}{|\boldsymbol{k}_\alpha|} \right)^{n-2}. \qquad (12.61)
$$

Here j_α is the flavor of the parton initiating collinear subgraph $C_{(\alpha)}$, k_α is the total momentum entering $C_{(\alpha)}$, and k_S is the total momentum entering the soft subgraph S; these momenta are also the total final-state momenta of the subgraphs. The hard subgraph H depends on the parton flavors and on the approximated momenta. Recall that the approximated $\hat{k}_\alpha$ is k_α projected by (12.57b) in a light-like direction appropriate for collinear subgraph $C_{(\alpha)}$. The dependence of S on parton flavors j_α is only through the color of the partons (3 v. $\bar{3}$ v. 8).

In the final form of factorization, (12.13), we treat the hard scattering as behaving like a cross section at the partonic level. For this purpose it is convenient to change variables in (12.61) from k_α to $\hat{k}_\alpha$, and so we need to take account of the Jacobian of the transformation.

For the first collinear group, the axes w_1 and $\tilde{w}_1$ are determined by the detected hadron, so we simply write

$$
\mathrm{d}^n k_1 = \mathrm{d} k_1^+ \, \mathrm{d} k_1^- \, \mathrm{d}^{n-2} \boldsymbol{k}_{1\,\mathrm{T}} = \mathrm{d}\hat{k}_1^+ \, \mathrm{d} k_1^- \, \mathrm{d}^{n-2} \boldsymbol{k}_{1\,\mathrm{T}}. \qquad (12.62)
$$

Here we define light-front coordinates with respect to w_1 and $\tilde{w}_1$: $k_1^+ = k_1 \cdot \tilde{w}_1$ and $k_1^- = k_1 \cdot w_1$. Now the only dependence in (12.61) on k_1^- and $\boldsymbol{k}_{1\,\mathrm{T}}$ is in the collinear subgraph $C_{(1)}$ itself. So we can short-circuit the integrals over these variables, restricting them to $C_{(1)}$. This will enable us to convert $C_{(1)}$ to a fragmentation function defined with light-front annihilation and creation operators, just as we did for parton densities. The integral over $\hat{k}_1$ gives the integral over z in the final factorization formulae, (12.13) and (12.21).

In contrast, the other collinear graphs have no fixed axes; the direction w_α is determined by the total final-state momentum k_α itself, which is an integration variable. So we perform a change of variable:

$$\mathrm{d}^n k_\alpha = \frac{\mathrm{d}^{n-1}\hat{\boldsymbol{k}}_\alpha}{2|\hat{\boldsymbol{k}}_\alpha|} 2k_\alpha^+ \, \mathrm{d}k_\alpha^- \left(\frac{|\boldsymbol{k}_\alpha|}{|\hat{\boldsymbol{k}}_\alpha|} \right)^{n-2}, \tag{12.63}$$

where the light-front variables are now those *local to* $C_{(\alpha)}$:

$$\hat{k}_\alpha^+ = k_\alpha^+ = k_\alpha \cdot \tilde{w}_\alpha = \frac{k_\alpha^0 + |\boldsymbol{k}_\alpha|}{\sqrt{2}} = \sqrt{2}|\hat{\boldsymbol{k}}_\alpha|, \tag{12.64a}$$

$$k_\alpha^- = k_\alpha \cdot w_\alpha = \frac{k_\alpha^0 - |\boldsymbol{k}_\alpha|}{\sqrt{2}}. \tag{12.64b}$$

The first factor on the r.h.s. of (12.63) is just the Lorentz-invariant phase space for a massless parton out of the hard scattering. We will use the integral over k_α^- to convert $C_{(\alpha)}$ into a light-cone object, similarly to the fragmentation function. The hard scattering is independent of k_α^-. However, the final factor in (12.63) arises from the Jacobian for the change of variables, and it introduces extra dependence on k_α^-.

We now see the reason for introducing the extra factor in the definition (12.59) of the hard factor. It is to cancel the inverse factor in (12.63). At this point we functionally differentiate with respect to the test function f, to obtain a factorized form

$$W^{\mu\nu}(q, p) = \int \mathrm{d}\hat{k}_1^+ \sum_{j_1} \left[\int \frac{\mathrm{d}k_1^- \, \mathrm{d}^{n-2}\boldsymbol{k}_{1\,\mathrm{T}}}{(2\pi)^n} C_{(1),j_1}(k_1, p) \right]$$

$$\times \prod_{\alpha=2}^N \sum_{j_\alpha} \int \frac{\mathrm{d}^{n-1}\hat{\boldsymbol{k}}_\alpha}{2|\hat{\boldsymbol{k}}_\alpha|(2\pi)^{n-1}} \prod_{\alpha=2}^N \left[2k_\alpha^+ \int \frac{\mathrm{d}k_\alpha^-}{2\pi} C_{(\alpha),j_\alpha}(k_\alpha) \right]$$

$$\times \int \frac{\mathrm{d}^n k_S}{(2\pi)^4} S_{j_1,\ldots j_\alpha}(k_S)(2\pi)^n \delta^{(n)}\left(q - \sum_{\alpha=1}^N \hat{k}_\alpha \right) H_{j_1,\ldots j_\alpha}(\hat{k}_1, \ldots, \hat{k}_N). \tag{12.65}$$

12.8.6 Soft cancellation

The soft factor in (12.65) and Fig. 12.12 has an unrestricted sum over cuts, and an unweighted integral over its external momentum k_S. I will now show that the result is zero. One possible argument uses the methods of Sec. 12.7. But instead, we use a simpler argument relying on properties of the Wilson lines in the soft factor's operator definition.

There is a slight complication because of UV divergences. As we know from Ch. 10, there is a multiplicative renormalization to make finite virtual graphs for the soft factor. Because of the integral over all k_S, in (12.65), real-emission graphs for the soft factor also acquire logarithmic UV divergences, which need to be renormalized. Our proof that the soft factor is unity will initially apply to the bare soft factor. The result for the bare factor implies that the UV divergences also cancel between real and virtual corrections.

On each side of the final-state cut we have a product of Wilson lines all going out from the same point to infinity. Because of the integral over *all* k_S the common point is the same on both sides of the cut. Thus the integrated soft factor is

$$S_{0,\text{integrated}} \stackrel{\text{def}}{=} \int \mathrm{d}^n k_S \, S = \left\langle 0 | M_1 T \left(\prod_\alpha W_{R(j_\alpha)}(+\infty, 0; n_\alpha) \right) \right.$$

$$\left. \times \bar{T} \left(\prod_\beta W_{R(j_\beta)}(+\infty, 0; n_\beta)^\dagger \right) M_2 |0\rangle \right. \tag{12.66}$$

Here M_1 and M_2 are the color matrices coupling the soft factor to the hard factor. The Wilson line $W_{R(j_\alpha)}(+\infty, 0; n_\alpha)$ goes from the origin towards infinity in direction n_α and has the color representation $R(j_\alpha)$ corresponding to collinear subgraph $C_{(\alpha)}$ with its parton of flavor j_α. The color index at its right-hand end (at infinity) couples to the corresponding index of the conjugate Wilson line $W_{R(j_\alpha)}(+\infty, 0; n_\alpha)^\dagger$.

The Wilson lines are space-like, so the time-ordering and anti-time-ordering prescriptions give the same results, since gluon fields commute at space-like separation. Then the Wilson lines cancel: $W_{R(j_\alpha)}(+\infty, 0; n_\alpha) W_{R(j_\alpha)}(+\infty, 0; n_\alpha)^\dagger = 1$, and the bare soft factor (12.66) is unity. Although there are UV divergences in individual cut Feynman graphs, the divergences cancel in the sum over all graphs and cuts. Therefore no overall minimal-subtraction counterterms are needed, and the renormalized soft factor is also unity.

As explained in a similar case in Ch. 10, the collinear factors are equipped with soft subtractions, and the collinear factor is the product of an unsubtracted collinear factor and a soft factor related to (12.66). Again the complete soft factor is integrated over all momentum, so it gives unity; thus the collinear factors are effectively unsubtracted.

12.8.7 Collinear cancellation

For each of the collinear factors $C_{(2)}, \ldots, C_{(N)}$ without a measured hadron, we have an unrestricted sum over cuts, and then an integral over k_α^-:

$$2k_\alpha^+ \int \mathrm{d}k_\alpha^- \quad \text{} \tag{12.67}$$

Here, $k_\alpha^\pm$ refers to components defined in local light-front coordinates, (12.64).

We now show that there is a suppression of (12.67) in the collinear region it was designed to treat. At first sight, it would be sufficient to appeal to the sum-over-cuts argument of Sec. 12.7. Indeed this argument works in a non-gauge theory, where we just have cut graphs for a full parton propagator, as in (12.50). We found that in each of the terms on the r.h.s. of (12.50) the k_α^- contour is not trapped. Thus we could deform the integral over k_α^- to a semicircle at infinity, to obtain a purely UV contribution.

This argument is broken by the Wilson lines in (12.67), for a somewhat non-trivial reason. The Wilson lines on the left and right of the final-state cut carry any value of momentum; loop momenta circulate freely through them. To make the sum-over-cuts argument work, we must also include a double line to continue the Wilson line across the final-state cut:

$$(12.68)$$

But to agree with the calculation in (12.67), the cut Wilson line must carry exactly zero 4-momentum, i.e., a cut Wilson line with momentum k' must be defined to have the value $(2\pi)^n \delta^{(n)}(k')$. In contrast, to apply the sum-over-cuts argument, the cut line needs to obey

$$= \frac{i}{k' \cdot \tilde{w}_\alpha + i0} + \frac{-i}{k' \cdot \tilde{w}_\alpha - i0}$$

$$= 2\pi\delta(k' \cdot \tilde{w}_\alpha)$$

$$(12.69)$$

That is, although the delta function forces one component of k', viz., $k' \cdot \tilde{w}_\alpha$, to be zero, the other components can have any value.

We solve this problem in two stages. First we show that if the quantity defined in (12.67) is integrated over $\boldsymbol{k}_{\alpha T}$, then the cut Wilson line can be treated as being given by (12.69). The resulting quantity, (12.68), is one to which the sum-over-cuts argument can be applied, so that it gives no trap of the integration momentum in a non-UV region. The second stage of the argument is to deduce that when the collinear quantity without the transverse-momentum integral is inserted in the factorization formula, there is a power-suppression of the collinear region.

When we use an integral over $\boldsymbol{k}_{\alpha T}$ as well as k_α^- applied to the cut graph in (12.67), we can choose to route these momenta through the cut Wilson line. As we explained, the cut Wilson line at this point is effectively replaced by $(2\pi)^n \delta^{(n)}(k')$. We apply $n-1$ dimensions of the delta functions to the integrations over $\boldsymbol{k}_{\alpha T}$ and k_α^-. The rest of the Wilson line does not depend on these two variables. There remains in the cut Wilson line the factor $2\pi\delta(k' \cdot \tilde{w}_\alpha) = 2\pi\delta(k'^+)$, which is just the rule (12.69) that we needed to use the sum-over-cuts argument. What we have just shown is that the integral of (12.67) over $\boldsymbol{k}_{\alpha T}$ is exactly the cut diagram (12.68) without any external integral at all. What was an external

integral over $\boldsymbol{k}_{\alpha \mathrm{T}}$ and k_α^- is now an internal loop integral routed from the $C_{(\alpha)}$ part of the graph back across the cut Wilson line.

The resulting quantity, which we will call $D_{(\alpha)}$, depends only on k_α^+, and the sum-over-cuts argument, as in Sec. 12.7, converts it to a difference of uncut amplitudes,

$$
D_{(\alpha)} \quad = \quad \text{} \quad + \quad \text{} \tag{12.70}
$$

and for each term there is no trapping of the momentum integration in the collinear region.

But this result is not sufficient for our purposes, since we defined coordinates for the collinear subgraph with respect to its final-state momentum (without the Wilson line). Thus $\boldsymbol{k}_{\alpha \mathrm{T}}$ is actually fixed at zero in the factor $C_{(\alpha)}$ in the factorization result (12.65). Now, at an exact collinear limit, transverse momenta are zero. The cancellation of collinear singularities in the integrated quantity (12.70) is between terms that have final states that differ by a shift in transverse momentum, which vanishes in the collinear limit. In the factorization formula (12.65) there is an integral over the center-of-mass angles of the collinear graphs $C_{(2)}, \ldots,$ $C_{(N)}$, and the remaining angular dependence is smooth dependence in the hard factor. This is sufficient to get the desired collinear cancellation.

The overall result is that the only genuinely collinear factor is $C_{(1)}$, which contains the detected hadron. The rest of the graph can be treated as making a hard subgraph. A more direct proof would be desirable.

12.8.8 Definitions of fragmentation functions

From the approximant for attaching the subgraph $C_{(1)}$ to the hard subgraph, we obtain the operator definitions of the fragmentation functions. The operators are the same as in parton densities (Sec. 7.5), since the approximants are the same. The normalizations are the same as in non-gauge theories, and therefore correspond to a number density interpretation.

We define the bare fragmentation function for a quark of flavor j by

$$
\begin{aligned}
d_{(0)\, h/j}(z) = {} & \frac{\text{Tr}_{\text{color}}}{N_{c,\,j}} \frac{\text{Tr}_{\text{Dirac}}}{4} \sum_X z^{n-3} \int \frac{\mathrm{d}x^-}{2\pi} e^{ik^+ x^-} \\
& \times \gamma^+ \langle 0 | \, \bar{T} \, W(\infty, x^-/2; \tilde{w}_1) \, \psi_j^{(0)}(x/2) \, | p, X, \text{ out} \rangle \\
& \times \langle p, X, \text{ out}| \, T \, \bar{\psi}_j^{(0)}(-x/2) \, W(\infty, -x^-/2; \tilde{w}_1)^\dagger \, | 0 \rangle
\end{aligned}
$$

$$
= \frac{\text{Tr}_{\text{color}}}{N_{c,\,j}} \frac{\text{Tr}_{\text{Dirac}}}{4} z^{n-3} \int \frac{\mathrm{d}k^- \, \mathrm{d}^{n-2}\boldsymbol{k}_{\mathrm{T}}}{(2\pi)^n} \gamma^+ \quad \text{} \tag{12.71}
$$

where $x^\mu = (0, x^-, \boldsymbol{0}_{\mathrm{T}})$. The Fourier transform implements the integral over $\boldsymbol{k}_{1\,\mathrm{T}}$ and k_1^-, and we now drop the subscript "1" on the external momentum of $C_{(1)}$.

This definition differs from that in a non-gauge theory, (12.40), only by having a Wilson line going out to future infinity in the light-like direction $\tilde{w}_1$ from the quark field. In principle, there are rapidity divergences associated with the light-like Wilson line and these are to be canceled by appropriate subtractions, which amount to a soft factor in the fragmentation function. But according to Sec. 12.8.6 this soft factor is unity, so that rapidity divergences cancel. This happens since we integrated over all transverse momentum.

When we go to the physical dimension $n = 4$, there are UV divergences, which we define to be renormalized away. Thus the final definition of the finite renormalized fragmentation function is given by (12.15), with the QCD definitions of bare fragmentation functions.

The antiquark fragmentation function is defined similarly.

The bare gluon fragmentation function is

$$
d_{(0)\,h/g}(z) = \frac{z^{n-3}}{N_{c,\,\text{gluon}}(n-2)k^+} \sum_X \int \frac{\mathrm{d}x^-}{2\pi} e^{ik^+x^-}
$$
$$
\times (-g_{\lambda\lambda'}) \langle 0 | \, G_{(0),\,b}^{+\lambda}(-x/2) \, \left[W_A(\infty, -x^-/2; \tilde{w}_1)^\dagger \right]_{bc} | p, X, \text{ out} \rangle
$$
$$
\times \langle p, X, \text{ out} | \, \left[W_A(\infty, x^-/2; \tilde{w}_1) \right]_{cd} \, G_{(0),\,d}^{+\lambda'}(-x/2) | 0 \rangle , \qquad (12.72)
$$

with again renormalization to be applied by (12.15). The field strength tensor $G^{+\lambda}$ is used for the same reason explained in Sec. 11.3 for the gluon density: it corresponds to a collinear G gluon, (11.6), attaching to the hard scattering. Since $G^{++} = 0$, the only terms in the Lorentz trace are for transverse indices. Then the overall factor $1/(n-2)$ in (12.72) gives an average over transverse gluon polarizations. The Wilson lines W_A are of course in the adjoint representation appropriate for gluons.

Feynman rules for the above definitions can be read off those for parton densities, with minor obvious variations. Renormalization is applied, leading to DGLAP equations, as stated in Sec. 12.2.2, with the derivations being like those for parton densities, Sec. 11.4.

12.8.9 Final state in fragmentation function

The final state $|p, X, \text{ out}\rangle$ in the fragmentation functions has non-zero color, because the field that creates it has color. This is obviously a wrong situation non-perturbatively in a confining theory. A full resolution of the issue has not appeared in the literature. But the following remarks suggest a possible approach.

The Wilson line represents a color source moving in the opposite direction to the parton initiating the fragmentation function. The color source is non-dynamical, moving along a fixed line, so let us call it a pseudo-parton. In the definition of a fragmentation function we treat the operator on the right as creating a state consisting of a parton and a pseudo-parton in an overall color singlet state. The pseudo-parton propagates to future infinity in the opposite direction to the jet that we can consider as being initiated by the regular parton. Then the final state consists of the ordinary hadrons in the jet, and at the opposite end a pseudo-meson consisting of the pseudo-parton and a regular parton. There are in addition some hadrons of intermediate rapidity. In some sense we consider the state space of QCD to include states of pseudo-partons.

12.8.10 Final result for factorization

Using these definitions of the renormalized fragmentation functions, together with the cancellation in the soft factor, we convert the factorization formula (12.65) to the form already stated in (12.13), (12.21), and (12.24). The factorization formula has the same form as in a non-gauge theory. However, the derivation was much more complicated.

12.9 Use of perturbative calculations

To apply the factorization formalism phenomenologically, we need perturbative calculations of the hard-scattering coefficients and of the evolution kernels of the fragmentation functions. These are independent of the choice of the detected particle. So, as explained in Sec. 9.3.1 for DIS, a convenient method of calculation is to choose the detected particle to be an on-shell quark or gluon, and then to perform low-order perturbative calculations of the hadronic tensor $W^{\mu\nu}$ and of the fragmentation functions. The factorization formula and the evolution equations allow us to deduce hard-scattering coefficients and the evolution kernels.

We perform these calculations with masses set equal to zero, and with dimensional regularization applied. There are soft and collinear divergences at the physical space-time dimension, but the divergences cancel in the hard scattering and the evolution kernels.

12.10 One-loop renormalization of fragmentation function

In this section I summarize one-loop calculations of the fragmentation functions for massless partons. We will deduce the renormalization of the fragmentation functions, from which follows the DGLAP kernels. At one-loop order, these are in fact equal to those for the parton densities. The calculations will also be used in the subtractions in calculations of the hard-scattering coefficients, Sec. 12.11.

12.10.1 Quark in gluon

There is one graph, Fig. 12.16, for the fragmentation function of a gluon into a quark. From the Feynman rules (cf. Fig. 7.12) for (12.72) we get

$$
\frac{g^2}{16\pi^2} d^{[1]}_{q/g}(z) = \frac{g^2 \mu^{2\epsilon} z^{1-2\epsilon}}{N_{c,g}(2-2\epsilon)(2\pi)^{4-2\epsilon}} \int dk^- d^{2-2\epsilon} \mathbf{k}_{\mathrm{T}} \, \frac{(2\pi)\delta\big((k-p)^2\big)}{(k^2)^2}
$$

$$
\times \operatorname{Tr} t_\alpha t_\alpha \operatorname{Tr}\left[-k^+ \not{p}\gamma^\mu (\not{k}-\not{p})\gamma_\mu + \not{p}\not{k}(\not{k}-\not{p})\gamma^+ \right.
$$

$$
\left. + \not{p}\gamma^+(\not{k}-\not{p})\not{k} - \frac{k^2}{k^+}\not{p}\gamma^+(\not{k}-\not{p})\gamma^+ \right] + \text{UV counterterm}
$$

$$
= \frac{g^2 T_F (4\pi\mu^2/z^2)^\epsilon}{8\pi^2 \Gamma(1-\epsilon)} \left[1 - \frac{2z(1-z)}{1-\epsilon} \right] \int_0^\infty dk_{\mathrm{T}}^2 (k_{\mathrm{T}}^2)^{-1-\epsilon} + \text{UV c.t.} \quad (12.73)
$$

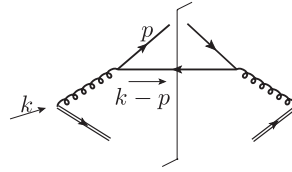462   *Fragmentation functions*

Fig. 12.16. One-loop Feynman graph for fragmentation function of quark in gluon.

Here the superscript "[1]" denotes "one-loop", and the group-theory factor is $T_F = \frac{1}{2}$ in QCD. The integral in the last line is zero. Being scale-free, it has a cancellation between equal and opposite divergences at zero and infinite k_{T}. The counterterm is computed from the large k_{T} part, giving

$$\frac{g^2}{16\pi^2} L_{q/g}^{[1]}(z) = -\frac{g^2 T_F [z^2 + (1-z)^2]}{8\pi^2} \frac{S_\epsilon}{\epsilon},\tag{12.74}$$

in the notation of (12.15), with S_ϵ given in (A.41).

This is also the UV-renormalized value of the fragmentation function:

$$\frac{g^2}{16\pi^2} d_{q/g}^{[1]}(z) = -\frac{g^2 T_F [z^2 + (1-z)^2]}{8\pi^2} \frac{S_\epsilon}{\epsilon}.\tag{12.75}$$

This exhibits the collinear divergence in the massless fragmentation function, and will be used in a subtraction term for the hard-scattering coefficient $C_g^{\mu\nu}$.

12.10.2 Quark in quark

The one-loop graphs for the fragmentation function of a quark into a quark are shown in Fig. 12.17. All are diagonal in quark flavor.

Graph (a)

This is

$$\frac{g^2}{16\pi^2} d_{q(j')/q(j)}^{[1,a]}(z) = \frac{g^2 \mu^{2\epsilon} \delta_{j'j} z^{1-2\epsilon}}{4 N_{c,q} (2\pi)^{4-2\epsilon}} \int \mathrm{d}k^- \, \mathrm{d}^{2-2\epsilon} \boldsymbol{k}_{\mathrm{T}} \, (2\pi)\delta\big((k-p)^2\big)$$

$$\times \frac{-\operatorname{Tr} \gamma^+ \slashed{k} \gamma^\mu \slashed{p} \gamma_\mu \slashed{k}}{(k^2)^2} \operatorname{Tr} t_\alpha t_\alpha + \text{UV counterterm}$$

$$= \frac{g^2 C_F \, \delta_{j'j} \, (4\pi\mu^2)^\epsilon}{8\pi^2} \frac{(1-\epsilon)(1-z)z^{-2\epsilon}}{\Gamma(1-\epsilon)}$$

$$\times \int_0^\infty \mathrm{d}k_{\mathrm{T}}^2 (k_{\mathrm{T}}^2)^{-1-\epsilon} + \text{UV c.t.}\tag{12.76}$$

The minus sign in the Dirac trace is from the numerator of the gluon propagator. Again, the value of the integral is zero, while canceling its UV divergence gives the counterterm:

$$\text{UV c.t. of (a)} = -\frac{g^2 C_F \, \delta_{j'j} \, (1-z)}{8\pi^2} \frac{S_\epsilon}{\epsilon}.\tag{12.77}$$

https://doi.org/10.1017/9781009401845.012 Published online by Cambridge University Press
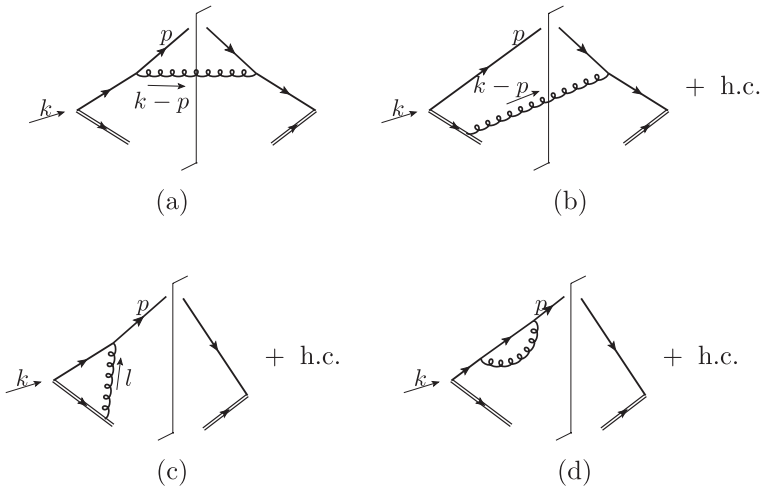
Fig. 12.17. One-loop Feynman graphs for fragmentation function of quark in quark; "h.c." means "hermitian conjugate".

Graph (b)

To make the relation to the Feynman rules for the Wilson line explicit, I write graph (b) in more detail, listing the individual propagators and vertices.

$$
\frac{g^2}{16\pi^2} d_{q(j')/q(j)}^{[1,b]}(z) = \frac{g^2 \mu^{2\epsilon} \, \delta_{j'j} \, z^{1-2\epsilon}}{4N_{c,q}\,(2\pi)^{4-2\epsilon}} \int dk^- \, d^{2-2\epsilon} \boldsymbol{k}_{\mathrm{T}}
$$

$$
\times \underset{\substack{\text{Dirac color}}}{\mathrm{Tr}\,\mathrm{Tr}} \; \gamma^+ \frac{i}{k^+ - p^+}(igt_\alpha g^{\mu+}) \, \not{p} \, (-igt_\alpha)^\dagger \gamma^\nu \frac{-i\not{k}}{k^2 - i0}
$$

$$
\times (-g_{\mu\nu})(2\pi)\delta\big((k-p)^2\big) + \text{UV counterterm}
$$

$$
= \frac{g^2 C_F \, \delta_{j'j} \,(4\pi\mu^2)^\epsilon z^{-2\epsilon}}{8\pi^2 \Gamma(1-\epsilon)} \frac{z}{1-z} \int_0^\infty dk_{\mathrm{T}}^2 (k_{\mathrm{T}}^2)^{-1-\epsilon} + \text{UV c.t.} \quad (12.78)
$$

Notice that the Wilson line has a vertex igt_α rather than $-igt_\alpha$, because it corresponds to an outgoing *anti*-triplet object. There are reversed $i0$s on the right of the final-state cut, as usual. The rapidity divergence of this graph manifests itself in the $1/(1-z)$ singularity, which gives a divergence when the graph is integrated with a test function $f(z)$. The hermitian-conjugate graph gives the same value. The UV counterterm for the two graphs is

$$
\text{UV c.t. of (b)+(b)}^\dagger = -\frac{g^2 \delta_{j'j} C_F}{4\pi^2} \frac{z}{1-z} \frac{S_\epsilon}{\epsilon}, \quad (12.79)
$$

Remainder of calculation

The virtual graph (c) involving the Wilson line has the same expression as the corresponding graph in the parton-density calculation (9.11). The value of the graph is again zero. In the

UV counterterm there is an integral over the momentum fraction α of the quark, and the integral has a divergence at $\alpha = 1$.

Finally, also exactly as in the parton-density calculation, the self-energy graph gives a zero contribution. But to get a correctly renormalized fragmentation function we add a contribution from the wave-function renormalization factor.

To see the expected cancellation of the rapidity divergence between real and virtual corrections, we use an integration with a test function, as in Sec. 9.4.4, after which the $1/(1-z)$ singularity becomes a plus distribution. The result for the counterterm is

$$\frac{g^2}{16\pi^2} L_{q/q}^{[1]}(z) = -\frac{g^2}{16\pi^2} C_F \frac{S_\epsilon}{\epsilon} \left[-\frac{4}{(1-z)_+} + 2 + 2z - 3\delta(z-1) \right]. \quad (12.80)$$

This is also the value of the graphs plus counterterms, to be used in subtractions in the hard scattering.

12.10.3 Gluon in quark, and gluon in gluon

The one-loop fragmentation functions to a gluon, $d_{g/q}^{[1]}(z)$ and $d_{g/g}^{[1]}(z)$, can be computed similarly. The calculation is left as an exercise.

12.10.4 DGLAP kernels

The one-loop renormalization counterterms are exactly the same for the fragmentation functions as those we calculated in Sec. 9.4 for the parton densities. It follows that the DGLAP evolution kernels are the same, so that the values in (9.6), (9.23), (9.24), and (9.25) also apply to fragmentation functions.

This relation does not hold at higher order. For the two-loop values see Furmanski and Petronzio (1980); Curci, Furmanski, and Petronzio (1980); Floratos, Kounnas, and Lacaze (1981); Kalinowski, Konishi, and Taylor (1981); Kalinowski *et al.* (1981). Note that there are misprints in the published version of Furmanski and Petronzio (1980).

12.11 One-loop coefficient functions

I now summarize a calculation of the one-loop coefficient functions for $e^+ e^- \to hX$. The calculation is phenomenologically significant, and it will also illustrate the principles to be applied.

Thus let $W_{\text{partonic } j}^{\mu\nu}$ be defined like the hadronic tensor, but with the detected particle being an (on-shell) massless parton of flavor j, so that the process is $e^+ e^- \to jX$. This object exists if we restrict ourselves to perturbation theory and use dimensional regularization to regulate the collinear and soft divergences. Factorization (12.21) gives

$$W_{\text{partonic } j}^{\mu\nu}(p, q) = \sum_{j'} \int_{x-}^{1+} \frac{\mathrm{d}z}{z^2} \, d_{j/j'}(z; \mu) \, C_{j'}^{\mu\nu}(\hat{k}, q; g(\mu), \mu). \quad (12.81)$$

Both $W^{\mu\nu}_{\text{partonic } j}$ and the partonic fragmentation functions can be computed from Feynman rules. From the expansion to one loop, we find

$$W^{[1]\,\mu\nu}_{\text{partonic } j}(p,q), = \sum_{j'} \frac{1}{x} d^{[1]}_{j/j'}(x;\mu)\, \tilde{C}^{[0]\,\mu\nu}_{j'}(p/x,q) + C^{[1]\,\mu\nu}_{j}(p,q), \qquad (12.82)$$

where the superscripts "[0]" and "[1]" denote the order of perturbation theory, and $\tilde{C}^{[0]}$ denotes the lowest-order coefficient function (12.26) *without* its $\delta(x/z-1)$ factor. From this we see that the one-loop coefficient function is its unsubtracted counterpart $W^{[1]\,\mu\nu}_{\text{partonic } j}$ minus a one-loop partonic fragmentation function, as calculated in Sec. 12.10. The formula is easily converted to one for the structure functions F_1 and F_2.

For $W^{[1]\,\mu\nu}_{\text{partonic } j}(p,q)$, the graphs are exactly the same as for the calculation of the e^+e^- annihilation total cross section in Sec. 4.2. We simply have to remove the integral over the momentum of the detected parton, adjusting the normalization to be that of $W^{\mu\nu}$.

Thus for the case of the inclusive production of a quark, consider the real-gluon-emission graphs of Fig. 4.8(a) and (b), which previously gave (4.27). Now, we replace the 3-body phase-space integral (A.44) by

$$\frac{1}{4\pi} \int \prod_{i=2}^{3} \frac{\mathrm{d}^{3-2\epsilon}\boldsymbol{k}_i}{(2\pi)^{3-2\epsilon}2|\boldsymbol{k}_i|} (2\pi)^{4-2\epsilon} \delta^{(4-2\epsilon)}(q-p-k_2-k_3)f(\boldsymbol{p},\boldsymbol{k}_2,\boldsymbol{k}_3)$$

$$= \frac{(4\pi)^\epsilon Q^{-2\epsilon}}{32\pi^2\Gamma(1-\epsilon)}\text{Ang. avg.}\int_0^1 \mathrm{d}\alpha \big[(1-x)\alpha(1-\alpha)\big]^{-\epsilon} f(\boldsymbol{p},\boldsymbol{k}_2,\boldsymbol{k}_3). \qquad (12.83)$$

Here the quark momentum k_1 is replaced by p, and the scalar variables in (4.27) are written as $y_1 = 1-x$, $y_2 = x\alpha$, and $y_3 = x(1-\alpha)$. There also appears the factor $1/(4\pi)$ from the definition (12.3) of $W^{\mu\nu}$.

One way of simplifying the calculation is to use scalar projections of the hadronic tensor, $-g_{\mu\nu}W^{\mu\nu}$ and $p_\mu p_\nu W^{\mu\nu}$, from which can be deduced results for the structure functions and for $\mathrm{d}\sigma_T/\mathrm{d}x$ and $\mathrm{d}\sigma_L/\mathrm{d}x$. At the end of the calculation, the variable x will be replaced by x/z for use in the factorization formulae.

The details of the calculation are left as an exercise. The results, in the $\overline{\text{MS}}$ scheme, are given in Rijken and van Neerven (1997), where also the NNLO coefficients are calculated. The NLO coefficients were first calculated by Baier and Fey (1979); Altarelli *et al.* (1979).

The variables in (12.83) were suitable for the quark coefficient function. The antiquark coefficient function is equal. The gluonic coefficient function is obtained by applying the variables α and x to a different permutation of partonic momenta: $y_1 = x\alpha$, $y_2 = x(1-\alpha)$, and $y_3 = 1-x$. As in Fig. 4.8, the labels 1, 2, and 3 refer to the quark, antiquark, and gluon respectively.

12.12 Non-perturbative effects and factorization

Gupta and Quinn (1982) pointed out a problem with factorization in the case that QCD is replaced by a theory in which all the quarks are heavy. Initially a quark-antiquark pair that is produced in e^+e^- annihilation at large Q/M goes outward at almost the speed of light. If

the quark and antiquark were to hadronize into a jet of color-singlet hadrons, there would need to be production of quark-antiquark pairs in the color flux tube joining the pair. But since all quarks are heavy, this is a slow weak-coupling process, governed by $\alpha_s(M)$. At the same, the gluonic non-perturbative interaction is still effective, and will tend to bring the quark and antiquark back. In the language of Sec. 4.3.1, the elastic-spring picture would likely be a better approximation than the breakable-string picture that appears to be valid in real QCD with its light quarks. This would break factorization for the inclusive hadron cross section; for example the direction of the jet and the hadrons in it would not correspond to the direction of a parton produced at short distances.

Now our proof of factorization used the structure of momentum regions that is seen in perturbation theory. So an important issue of principle is to what extent non-perturbative effects change the results. This is a far-from-completely understood subject. It would seem best to consider the process in coordinate space. Then the breakable-string picture would appear to be compatible with preserving the factorization structure seen in perturbation theory.

This led Gupta and Quinn to an interesting question. Suppose an experimental test were made of a perturbatively calculated jet cross section or of a factorized hadron-production process such as we treated in this chapter, and suppose that experiment and theory substantially disagreed. Would this count as evidence against QCD? Gupta and Quinn argued cogently that it would not, by itself, falsify QCD. The reason is that they could show a counterexample where the theoretical methods are violated non-perturbatively without any problem with the perturbative calculations.

What would actually be falsified would be the combination of QCD and the (mostly implicit) assumptions about non-perturbative physics used in deriving factorization etc.

In the time since Gupta and Quinn (1982), there have be many successful comparisons of QCD predictions with data. So we should not count all of these successes as successful predictions of QCD itself. An isolated single experiment in this area does not test QCD. Some of the results should be counted as establishing the breakable-string picture. Then the other experiments can be regarded as QCD tests.

At the present time, one must regard QCD as being very well established. Failure of a comparison between QCD predictions and experiment is highly unlikely to impinge on QCD itself. Depending on the situation, much more likely situations would involve any or all of: (a) problems with the experiment itself, (b) problems with more exotic QCD methods, and (c) physics beyond the Standard Model.

12.13 Generalizations

Although the last part of the proof in Sec. 12.8 was specific to the one-particle-inclusive cross section, the bulk of it applies to much more general situations in e^+e^- annihilation.

12.13.1 Multiparticle cross sections

Consider an inclusive cross section differential in more than one hadron. We first suppose the particles are all at wide angles with respect to each other. In that case, in the
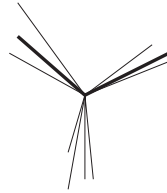
Fig. 12.18. Three-jet configuration with registered particles (thick lines) in two of the jets. The line lengths indicate momenta.

leading-region analysis, each of the particles arises from a different collinear subgraph. An example of such a final-state configuration is shown in Fig. 12.18.

We simply apply the same method of proof as for the single-particle-inclusive cross section. For each measured particle its collinear subgraph becomes a fragmentation function, and we have the factorization property

$$\frac{\mathrm{d}\sigma}{\prod_{\alpha=1}^{N_p}(\mathrm{d}^3\boldsymbol{p}_\alpha/E_{\boldsymbol{p}_\alpha})} = \prod_{\alpha=1}^{N_p}\left[\sum_{j_\alpha}\int\frac{\mathrm{d}z_\alpha}{z_\alpha^2}d_{h_\alpha/j_\alpha}(z_\alpha)\right]\frac{\mathrm{d}\hat\sigma_{\text{partonic, subtracted}}}{\prod_{\alpha=1}^{N_p}(\mathrm{d}^3\boldsymbol{k}_\alpha/E_{\boldsymbol{k}_\alpha})}, \qquad (12.84)$$

with hadron and parton 3-momenta related by $\boldsymbol{p}_\alpha = z_\alpha\boldsymbol{k}_\alpha$. We treat this as a partonic cross section convoluted with a number density for the partons to make the measured hadrons. As usual, the partonic cross section is subtracted.

Each of the fragmentation functions contains an integral over its parent parton's minus and transverse momentum (defined with respect to the hadron in the fragmentation function). As in the one-particle-inclusive cross section, we use approximated parton kinematics for the hard scattering. That works when the hadrons are at wide angle, since it is equivalent to a small shift in the hadronic momenta. For example a transverse momentum of order Λ corresponds to an angular shift of order Λ/Q.

(The reader may point out that the integral over partonic momenta also extends to large minus and transverse momenta, where the approximation is always bad. A reminder is needed that within the subtraction method, all that is necessary is that the approximant be accurate to order k_{T}/Q and k^-/Q for its design region. As the distance of momenta from the skeleton of some region R increases, so does the error in the region's approximant T_R. But, as illustrated in Sec. 10.2, the increasing errors are compensated by the terms for larger regions together with their double-counting subtraction terms.)

12.13.2 Back-to-back region

But when the detected hadrons are almost back-to-back, as in Fig. 12.19, the neglect of partonic transverse momentum in the hard scattering is no longer correct, even in the collinear region. The situation therefore needs a somewhat different kind of factorization, which we will treat in Ch. 13.

Alternatively, we can integrate over the angle between the measured particles, averaging over the back-to-back region with a suitably broad function. At this point, the neglect of
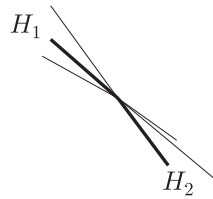
Fig. 12.19. Two-jet configuration with a registered particle (thick lines) in each jet.

partonic transverse momenta in the averaging function regains its accuracy in the collinear region, so that we can continue to use integrated fragmentation functions.

12.13.3 Multiparticle fragmentation

Another simple generalization is when two (or more) measured hadrons are approximately parallel. Then they come out of a single collinear subgraph.

This situation is dealt with by an elementary generalization (Konishi, Ukawa, and Veneziano, 1978) of the definitions of fragmentation functions. For example, consider the case of two measured hadrons of momenta p_1 and p_2. In the final state in a definition like (12.35), we replace $|p, X, \text{out}\rangle \langle p, X, \text{out}|$ by $|p_1, p_2, X, \text{out}\rangle \langle p_1, p_2, X, \text{out}|$. At the partonic end of the fragmentation function, nothing changes. So all the issues about renormalization, DGLAP evolution, and the construction of a hard-scattering coefficient function are unchanged. The fragmentation function becomes a function of more variables, representing the kinematics of p_1 and p_2 relative to the parton.

A significant use of this idea is in transverse-spin physics. With fragmentation to a single pion, there is no polarization dependence of the fragmentation function; only the unpolarized fragmentation functions are non-zero. But with two-particle fragmentation, a transversely polarized quark can give an azimuthal dependence of the form

$$A + B \cos \phi. \tag{12.85}$$

Here ϕ is the angle in the transverse plane between the transverse-spin vector of the quark and the normal to the plane of the two measured pions. The coefficient A is proportional to the ordinary unpolarized fragmentation function, while B is proportional to a kind of polarized fragmentation function that was proposed in Collins, Heppelmann, and Ladinsky (1994). It can be probed in e^+e^- annihilation, because there is a correlation of the transverse spins of the quark and antiquark in the lowest-order graph. Therefore the polarized dihadron fragmentation function appears in the factorization theorem for e^+e^- annihilation to four pions, with the pions grouped in two small-angle pairs (Artru and Collins, 1996). The function also appears in factorization for DIS with two measured hadrons in the final state when the target hadron is transversely polarized.

Data on the two-hadron fragmentation function have recently become available: Airapetian *et al.* (2008); Vossen *et al.* (2009); Wollny (2009). Fits have been made by Bacchetta *et al.* (2009).

12.13.4 Jet cross sections

For the e^+e^- annihilation total cross section to hadrons, we used a sum over all final states to get a perturbatively calculable IR-safe cross section. Similarly, in inclusive cross sections, we used a similar sum to obtain cancellations of IR-sensitive parts of the soft factor and of those collinear factors that did not couple to measured hadrons.

The cancellations involve collinear and soft interactions. In the exact collinear (or soft) limit, these interactions cause transitions between different final states with the same momentum. This suggests a general strategy to obtaining perturbatively calculability by defining IR-safe jet cross sections. These are computed from the angular pattern of energy flow, and do not depend on how the energy is split among particles.

A simple example is a calorimetric cross section (Sterman, 1996) in e^+e^- annihilation. Here we use a cross section weighted by a suitable function S of the momenta of the particles in the final state:

$$\sigma_S = \sum_n \int \mathrm{d}\tau_n \frac{\mathrm{d}\sigma}{\mathrm{d}\tau_n} S_n(p_1/Q, \ldots, p_n/Q), \qquad (12.86)$$

where n is the number of hadrons in the final state, and $\mathrm{d}\tau_n$ represents the element of n-body phase-space. The weight function S_n is defined for any n-body configuration.

The cancellations needed for IR safety of the cross section σ_S occur if (Sterman, 1996) "the weight function does not distinguish between states in which one set of collinear particles is substituted for another set with the same total momentum, or when zero-momentum particles are absorbed or emitted". Mathematically this is formulated as follows:

- The weighting functions are smooth.
- They are symmetric functions of their arguments.
- For massless momenta, they obey

$$S_n(p_1/Q, \ldots, p_i/Q, \ldots, p_{n-1}/Q, \lambda p_i/Q)$$
$$= S_{n-1}(p_1/Q, \ldots, p_i(1+\lambda)/Q, \ldots, p_{n-1}/Q), \qquad (12.87)$$

with λ being any real parameter $\lambda \geq 0$.

The weighting functions are defined to be functions of momenta scaled by Q. This matches the Libby-Sterman analysis, since the cancellations needed for IR safety occur in a fixed region of the scaled momenta. Smoothness of the weighting functions is needed because the necessary cancellations occur in a neighborhood of the massless PSS configurations.

In practice, two rather different approaches are used instead, which more directly probe the jet structure of final states. One is to define global measures of the jet structure of a final state. A classic example is thrust,[1] defined on an n-particle state by

$$T \overset{\mathrm{def}}{=} \frac{1}{\sum_i |\boldsymbol{p}_i|} \max_{\hat{\boldsymbol{n}}} \sum_{i=1}^n |\boldsymbol{p}_i \cdot \hat{\boldsymbol{n}}|, \qquad (12.88)$$

---

[1] The definition given here is the current standard one, and is based on a slightly different definition by Farhi (1977).

with the maximum being over unit 3-vectors $\hat{\boldsymbol{n}}$ in the overall center-of-mass frame. The direction that gives the maximum is called the thrust axis. Thrust has a maximum value of unity, when a final state has a perfect 2-jet configuration, i.e., some of the momenta are exactly aligned in one direction and the others are exactly aligned in the opposite direction. A spherically uniform distribution of momenta gives $T = \frac{1}{2}$.

Applying this definition of thrust as a weight function gives the average value of thrust, a measure of the average 2-jet-likeness of final states. Commonly a cross section *differential* in thrust is measured, e.g., Bethke *et al.* (2009). Showing that the differential thrust distribution is IR safe requires a generalization of the previous discussion.

Perhaps the most common approach is to define jets directly by grouping measured hadrons into clusters by some "jet algorithm". The clusters are labeled as jets, and cross sections differential in jet momenta are measured. In a leading-order approximation, a jet's momentum is close to its parent parton's momentum as in Fig. 2.3. It is quite non-trivial to determine whether a particular jet algorithm is IR safe. An important practical constraint is that the algorithm should be suitable for implementation both in experimental analyses and in theoretical calculations. See Salam (2010) for a recent review.

12.14 Semi-inclusive deeply inelastic scattering

Another classic process where fragmentation functions appear is semi-inclusive deeply inelastic scattering (SIDIS), i.e., DIS differential in one (or more) hadrons in the final state, e.g., $e(l) + P \rightarrow e(l') + \pi(p_h) + X$, Fig. 12.20.

12.14.1 Kinematics and structure functions

For the kinematics, we need to supplement the variables for DIS by a specification of the momentum of the outgoing hadron. In the Breit frame, we write

$$q = \left(-x P^+, \frac{Q^2}{2x P^+}, \mathbf{0}_{\mathrm{T}} \right), \tag{12.89a}$$

$$P = \left(P^+, \frac{M^2}{2 P^+}, \mathbf{0}_{\mathrm{T}} \right), \tag{12.89b}$$

$$p_h = \left(\frac{p_{h\,\mathrm{T}}^2 + m_h^2}{2 p_h^-}, p_h^-, \boldsymbol{p}_{h\,\mathrm{T}} \right). \tag{12.89c}$$

For the independent scalar variables of the hadronic part of the cross section, we use x and Q as usual, together with

$$z = \frac{P \cdot p_h}{P \cdot q} \simeq \frac{p_h^-}{q^-}, \qquad |\boldsymbol{p}_{h\,\mathrm{T}}|^2 \simeq z^2 Q^2 + 2zq \cdot p_h, \tag{12.90}$$

and the azimuthal angle ϕ_h of $\boldsymbol{p}_{h\,\mathrm{T}}$. The approximations in (12.90) are valid when masses can be neglected. The standard specification of the angle is given by the Trento convention (Bacchetta *et al.*, 2004); the angle is relative to the lepton plane: Fig. 12.21.
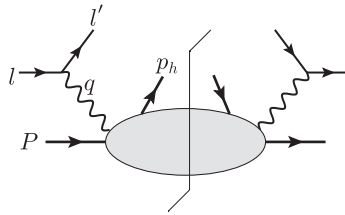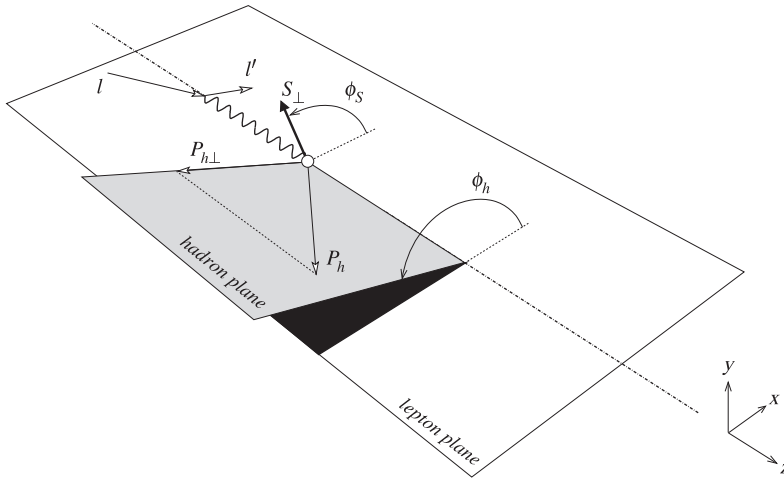
Fig. 12.20. SIDIS cross section.

Fig. 12.21. SIDIS kinematics, from Bacchetta *et al.* (2004). This diagram is given in the target rest frame, and gives the Trento convention for defining the azimuthal angles of the measured outgoing hadron and of the target's spin vector. (Copyright (2004) by The American Physical Society.)

The significance of the z variable is given in the parton-model approximation applied to Fig. 12.22. Viewed in the Breit frame, the outgoing quark is approximately light-like, $k + q \simeq (0, q^-, \mathbf{0}_T)$. Thus the experimentally measured variable z approximates the fractional momentum of the detected hadron relative to its parent quark, just as x approximates the fractional momentum of the struck quark k relative to the target hadron.

Given the basic meaning of a fragmentation function as a number density for a hadron in a parton-induced jet, we immediately deduce a parton-model formula for the cross section integrated over the transverse momentum $\boldsymbol{p}_{h\,T}$ of the detected hadron:

$$\frac{\mathrm{d}\sigma}{\mathrm{d}x\,\mathrm{d}y\,\mathrm{d}z} \simeq \frac{4\pi\alpha^2}{yQ^2}(1 - y + y^2/2)\sum_j e_j^2 f_j(x)d_{h/j}(z). \quad \text{(Parton model)} \qquad (12.91)$$

This is obtained by appending fragmentation functions to the parton model for inclusive DIS, from (2.22) and (2.29), with neglect of masses. As usual $y = q \cdot P / l \cdot P \simeq Q^2/(xs)$.
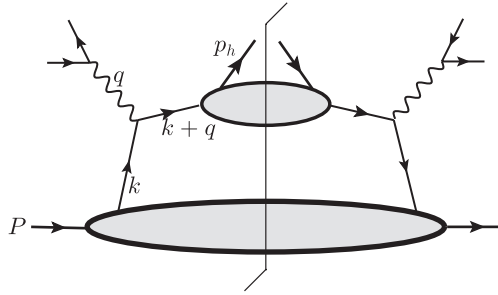
Fig. 12.22. Parton model for SIDIS.

A general structure function analysis is more complicated than for ordinary DIS, because of the extra vector. The details can be found in Bacchetta *et al*. (2007), which includes the important case of a polarized target. For experiments, the importance of the structure function analysis is that in the full differential cross section,

$$\frac{\mathrm{d}\sigma}{\mathrm{d}x \, \mathrm{d}y \, \mathrm{d}z \, \mathrm{d}p_{h\,\mathrm{T}} \, \mathrm{d}\phi_h}, \tag{12.92}$$

the azimuthal dependence is restricted to certain trigonometric functions. The simplest case is the unpolarized cross section, where the azimuthal dependence is of the form

$$A + B \cos\phi_h + C \cos 2\phi_h, \tag{12.93}$$

with the coefficients being functions of the other variables. The situation is more complicated for the polarized case, generalizing the same idea. The extra terms are each associated with certain polarized parton densities and fragmentation functions.

12.14.2 Leading regions

To derive factorization, we use the same sequence of steps as for e^+e^- annihilation. An important difference is in how a contour deformation is made to get out of the Glauber region; this will have particularly notable consequences when we treat situations needing transverse-momentum-dependent parton densities and fragmentation functions in Ch. 13.

The leading regions have a hard scattering on each side of the final-state cut, and the virtual photon is attached to the hard scattering. There are at least two collinear graphs, one of which includes the target. There may be a soft subgraph connecting by gluons to any of the collinear subgraphs. Each of the collinear subgraphs connects to each hard-subgraph amplitude by a primary parton line plus any number of Grammer-Yennie K-gluons. All this follows from the usual power-counting.

There are two classes of collinear subgraph: the target subgraph and what we will call hard-jet subgraphs. The "hard-jet" terminology associates them with the final state of a hard scattering. In the laboratory frame the associated regions have large transverse momentum, of order Q. In the brick-wall frame the associated regions either have large transverse
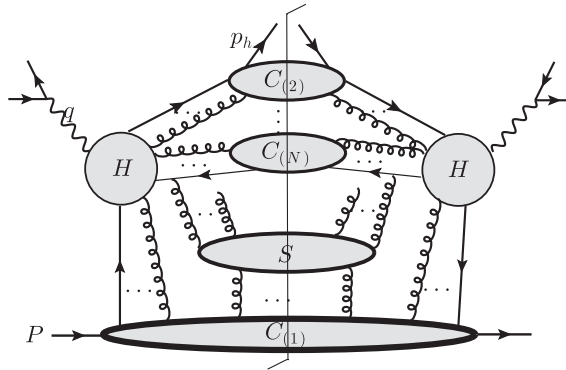
Fig. 12.23. Typical leading region for SIDIS, when the measured final-state hadron is in the "current fragmentation region". Three collinear subgraphs are shown; the minimum is two.
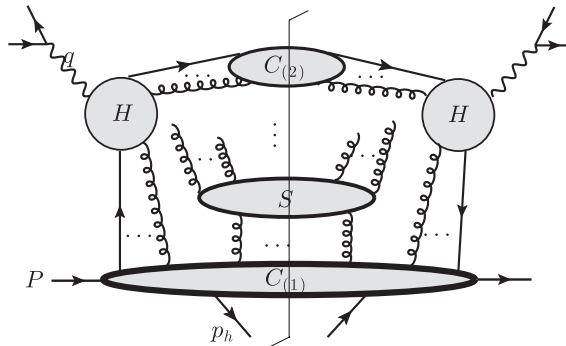

Fig. 12.24. Like Fig. 12.23, but when the measured final-state hadron is in the "target fragmentation region". Two collinear subgraphs are shown, but extra hard-jet subgraphs are also possible.

momentum or they have large minus momentum (appropriate for the parton model with a single hard jet).

Depending on its kinematics, the measured hadron either comes from a hard-jet subgraph, the target subgraph, or the soft subgraph.

When the hadron is from a hard jet, it is said to be in the "current fragmentation region", as shown in Fig. 12.23. When it is from the target subgraph, it is said to be in the "target fragmentation region", as shown in Fig. 12.24. The hadron comes from the target or soft subgraphs only when z is small, so that p_h^- is small. We can characterize a canonical situation for a target-collinear hadron by $z \sim m^2/Q^2$ and a soft hadron by $z \sim m/Q$.

For the rest of this section we will only be concerned with the current fragmentation region, $z \gg m/Q$. Target-collinear hadrons will be briefly discussed in Sec. 12.15. We will not treat soft measured hadrons at all.
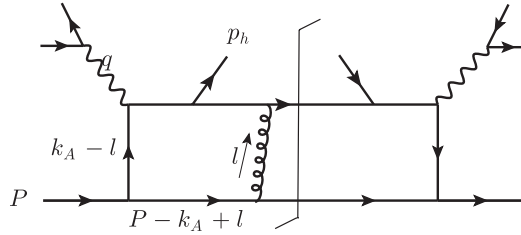
Fig. 12.25. Illustrating Glauber region for (SI)DIS.

12.14.3 Glauber region and (SI)DIS

The Ward-identity argument needed to factor the soft subgraph requires that the contour of integration over soft momenta avoid the Glauber region, i.e., that there be no pinch in the Glauber region. The general conditions for a pinch in a Glauber region were given in Sec. 5.6. They concern a pinch of the smallest components of soft momenta when they flow through collinear subgraphs.

The ability to do a suitable contour deformation is completely determined by examining low-order graphs. In e^+e^- annihilation, the collinear subgraphs are all in the final state relative to the hard scattering. So, as we saw in Sec. 10.6.4, we could deform exchanged Glauber momenta away from all the collinear singularities. For example, in an exchange between two collinear groups, the deformation would avoid the final-state singularities of both collinear groups.

In DIS, the situation is typified by Fig. 12.25, which represents a graph in a model for SIDIS. In contrast with e^+e^- annihilation, only a one-sided deformation works, to deform l^+ away from final-state singularities in the upper jet, but l^- is trapped in the target-collinear subgraph. Consider the region where the lower lines are target-collinear, with momenta of order $(Q, \lambda^2/Q, \lambda)$, the upper lines are the opposite collinear: $(\lambda^2/Q, Q, \lambda)$, while the gluon is Glauber: $l \sim (\lambda^2/Q, \lambda^2/Q, \lambda)$. The target lines trap l^- between initial- and final-state poles:

$$\frac{1}{[(k_A - l)^2 - m^2 + i0] \, [(P - k_A + l)^2 - m^2 + i0]}$$
$$\simeq \frac{1}{[-2k_A^+ l^- + \cdots + i0] \, [2(P^+ - k_A^+)l^- + \cdots + i0]}. \tag{12.94}$$

The approximation is valid when k_A is target collinear and l is soft or Glauber. The dots indicate terms that do not depend on l^-. The trapping of the l^- contour at values of order λ^2/Q is because on one line the direction of l is with the flow of plus momentum and on the other the line it is against. As to l^+, in the Glauber region the only significant dependence is in the upper two lines, where it always is in the opposite direction relative to the large outgoing collinear minus momentum. Thus l^+ is not trapped; we can deform the contour to much larger values of l^+. The deformation only stops when we get out of the Glauber region.

In order to make the region approximators, we must choose the auxiliary vectors (Sec. 10.6.4) for the K gluons so as not to obstruct the deformation. The space-like future-pointing vectors chosen in that section continue to work here.

12.14.4 Factorization for SIDIS

Once the contours are out of the Glauber region, we can copy the factorization proof for e^+e^- annihilation. We have applied approximants and subtractions for the contributions of each region of each graph, and sum over possibilities.

We first use Ward identities to extract collinear K gluons from the hard scattering, converting them to Wilson lines. Similarly we extract the soft gluons from the collinear subgraphs.

The sum-over-cuts argument applies to all the collinear subgraphs except for the target subgraph and the one to which the measured hadron attaches. Provided we average over a broad range of transverse momentum $\boldsymbol{p}_{h\,\mathrm{T}}$ for the measured hadron, we can also apply the sum-over-cuts argument to the soft subgraph. We are left with a hard subgraph convoluted with a parton density and a fragmentation function, which arise for the same reasons as in our factorization arguments separately for DIS and e^+e^- annihilation.

The resulting factorization theorem is conveniently stated in terms of a cross section differential in Lorentz-invariant phase-space, in a form generalizing (12.13):

$$E \frac{\mathrm{d}\sigma(e + P \to e + p_h + X)}{\mathrm{d}^3 \boldsymbol{p}_h} = \sum_{jj'} \int_{x-}^{1+} \frac{\mathrm{d}\xi}{\xi} \int_{z-}^{1+} \frac{\mathrm{d}\zeta}{\zeta^2} \, E_k \frac{\mathrm{d}\hat{\sigma}_{jj'}}{\mathrm{d}^3 \boldsymbol{k}} \, d_{h/j'}(\zeta; \mu) f_{j/P}(\xi; \mu).$$

$$(12.95)$$

The hard scattering is for a parton of flavor j and massless momentum $\xi \hat{P}$ to scatter inclusively to a parton of flavor j' and massless momentum $\hat{p}_h/\zeta$. Here the hatted momenta have the same 3-momenta as the unhatted momenta in the brick-wall frame, and have their energies set to make the momenta massless.

One can convert the above to a formula for the structure functions.

12.15 Target fragmentation region: fracture functions

When the detected final-state hadron is in the target-collinear region, the leading regions have the form shown in Fig. 12.24. There is a hard subgraph H, a target-collinear subgraph $C_{(1)}$, one or more hard-jet subgraphs $C_{(2)}, \ldots, C_{(N)}$ and a soft subgraph S. These are exactly like those for ordinary DIS, except that the target-collinear subgraph now contains the detected hadron. To specify the longitudinal kinematics of p_h, it is convenient not to use z, but instead a target-relative variable

$$x_h \stackrel{\text{def}}{=} \frac{p_h^+}{P^+} \simeq \frac{p_h \cdot q}{P \cdot q}.$$

$$(12.96)$$

Factorization can be derived by the same arguments we have already described. First, the soft subgraph can be factored out and then shown to cancel. The K gluons from the
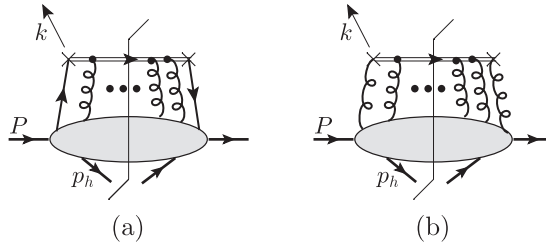
Fig. 12.26. Diagrammatic representation of gauge-invariant fracture functions. The partonic part, with its Wilson line, is the same as for parton densities in Fig. 7.9.

collinear subgraphs can be extracted from the hard subgraph, to give Wilson lines, after which the hard-jet subgraphs are of the form in which the integrations can be taken out of their collinear regions. We end up with exactly the same structure as in DIS. We have a hard scattering of identically the same form as in DIS, and it is convoluted with a target-collinear quantity whose definition is the same as a parton density, except that the final state is required to contain the detected hadron. These quantities are called "extended fracture functions" (Grazzini, Trentadue, and Veneziano, 1998). For the case of a bare quark fracture function, the definition, generalized from the quark density defined in (7.40), is (Berera and Soper, 1996)

$$M_{(0) jh/P}(x, x_h, \boldsymbol{p}_{h\,\mathrm{T}}) = \int \frac{\mathrm{d}w^-}{2\pi} e^{-ixP^+w^-} \sum_X \langle P|\overline{\psi}_j^{(0)}(0, w^-, \boldsymbol{0}_{\mathrm{T}})W(\infty, w^-)^\dagger|p_h, X, \ \mathrm{out}\rangle$$

$$\times \langle p_h, X, \ \mathrm{out}|\frac{\gamma^+}{2} W(\infty, 0)\psi_j^{(0)}(0)|P\rangle_{\mathrm{c}}, \qquad (12.97)$$

where the Wilson line (in the minus direction) was defined in (7.41). A similar modification to the definition of the gluon density gives the gluon fracture function. These definitions are shown diagrammatically in Fig. 12.26. In the unpolarized case, there is no preferred axis in the transverse plane, so the dependence on the transverse momentum of the detected hadron is only through its size.

Since the parton kinematics are treated identically to those of parton densities, the Feynman rules at the parton end are the same as for parton densities. Hence renormalization of extended fracture functions has the same form (8.11) as for parton densities. The DGLAP equations therefore have the same form as (8.30) for parton densities:

$$\frac{\mathrm{d}}{\mathrm{d}\ln\mu} M_{jh/P}(x, x_h, \boldsymbol{p}_{h\,\mathrm{T}}; \mu) = 2 \sum_{j'} \int \frac{\mathrm{d}z}{z} P_{jj'}(z; g) M_{j'h/P}(x/z, x_h, \boldsymbol{p}_{h\,\mathrm{T}}; \mu). \quad (12.98)$$

There is a kinematic constraint $x + x_h \le 1$, given by energy positivity for the unobserved part $|X\rangle$ of the hadronic final state.

The above functions are officially called "extended fracture functions", even though the term "fracture functions" would be more natural. However the latter term was already defined (Trentadue and Veneziano, 1994) to refer to similar quantities defined with an

integral over all $\boldsymbol{p}_{h\mathrm{T}}$. Because of the integral, these quantities also include contributions from the current fragmentation region and have more complicated evolution equations. It seems better to use only extended fracture functions.

The extended fracture functions can be notated as parton densities differential in p_h:

$$M_{jh/P}(x, x_h, \boldsymbol{p}_{h\mathrm{T}}) = (2\pi)^3 2E_{p_h} \frac{\mathrm{d}f_{jh/P}}{\mathrm{d}^3\boldsymbol{p}_h}. \qquad (12.99)$$

One way of stating the factorization theorem is to project the SIDIS cross section onto structure functions. These are like F_2 etc. for DIS, but now differential in x_h and $\boldsymbol{p}_{h\mathrm{T}}$:

$$\frac{\mathrm{d}F_2(x, Q^2; x_h, \boldsymbol{p}_{h\mathrm{T}})}{\mathrm{d}x_h\, \mathrm{d}^2\boldsymbol{p}_{h\mathrm{T}}}. \qquad (12.100)$$

Then factorization is a simple generalization of the version (8.83) for DIS:

$$\frac{\mathrm{d}F_1(x, Q^2; x_h, \boldsymbol{p}_{h\mathrm{T}})}{\mathrm{d}x_h\, \mathrm{d}^2\boldsymbol{p}_{h\mathrm{T}}} = \sum_j \int_{x-}^{1+} \frac{\mathrm{d}\xi}{\xi} \hat{F}_{1j}(Q/\mu, x/\xi; \alpha_s) \frac{M_{jh/P}(\xi, x_h, \boldsymbol{p}_{h\mathrm{T}})}{16\pi^3 x_h}, \quad (12.101\mathrm{a})$$

$$\frac{\mathrm{d}F_1(x, Q^2; x_h, \boldsymbol{p}_{h\mathrm{T}})}{\mathrm{d}x_h\, \mathrm{d}^2\boldsymbol{p}_{h\mathrm{T}}} = \sum_j \int_{x-}^{1+} \mathrm{d}\xi\, \hat{F}_{2j}(Q/\mu, x/\xi; \alpha_s) \frac{M_{jh/P}(\xi, x_h, \boldsymbol{p}_{h\mathrm{T}})}{16\pi^3 x_h}, \quad (12.101\mathrm{b})$$

valid up to power-suppressed corrections. The hard-scattering coefficients are the same as in ordinary DIS.

The primary phenomenological applications are to diffractive DIS on protons. This concerns the case that x_h is close to unity (with, necessarily, $x \ll 1$), and that the detected hadron is also a proton. See Chekanov *et al.* (2010) for recent results. In this case the extended fragmentation functions are commonly referred to as "diffractive parton densities".

Quite elementary extensions of these ideas can be applied to cross sections differential in more final-state hadrons. One example is the dijet cross section in diffractive DIS (Aktas *et al.*, 2007a), which is differential in one proton in the target fragmentation region and in two hard jets. Diffractive parton densities can be obtained from a fit to ordinary diffractive DIS, without the dijet condition. Then the cross section for diffractive dijet DIS is predicted with the aid of standard perturbative calculations for the hard scattering. The success of the prediction confirms the experimental validity of the factorization approach.

Exercises

12.1 (**) Find and prove any extensions to the Ward-identity arguments of Ch. 11 that are needed to apply them to the processes treated in this chapter.

12.2 (*****) Construct a good formalism for the evolution of states in space-time from a quark state to a hadronic state. Ideally, this should be a rigorous formalism from which you can derive from first principles that partonic states evolve to jet-like configurations. Publish your results.

Undoubtedly I have stated this (very difficult) problem quite badly, and part of the answer should be to formulate this problem more appropriately. A good solution

to this problem should answer the issues raised, for example, by Gupta and Quinn (1982). See problem 5.1 for some results that may be of use.

12.3 (**) In Sec. 12.12, I discussed whether non-perturbative effects can ruin factorization in inclusive cross sections in e^+e^- annihilation. Give a more detailed and explicit account of these issues by critically using the methods and results of Einhorn (1976, 1977).

In these papers Einhorn made approximate calculations in the model of large-N_c QCD in two space-time dimensions. The final states given by this model, both in e^+e^- annihilation and in DIS, are a series of closely spaced narrow resonances. Thus the model consistently realizes an approximately unbreakable elastic-spring picture. Einhorn found contrasting results relative to the parton model for different kinds of cross section: DIS, the total cross section for e^+e^- annihilation, and the single-hadron-inclusive process $e^+e^- \to \pi + X$.

Use these results to illustrate the non-perturbative properties that either preserve or violate factorization in the different reactions.

12.4 (**) Investigate the soft gluon cancellation in Figs. 12.7 and 12.8. Assume that the quark is approximately parallel to the modeled pion, that the antiquark moves in approximately the opposite direction, and that the gluon is soft. Show that there is a cancellation between all the graphs in Figs. 12.7 and 12.8. But show that the cancellation does not work if it is restricted to subsets of graphs related by sums-over-cuts, i.e.,
- between Fig. 12.7(a) and (b),
- between Fig. 12.7(c) and (d),
- between the graphs of Fig. 12.8 alone.

For sufficiently soft gluons, internal emission will be suppressed, and there will be a cancellation in Fig. 12.8 alone. But when the gluon momentum l becomes comparable to or larger than M^2/Q, internal line emission is important. Here M denotes the invariant mass of the upper jet.

12.5 (**) Complete the proofs sketched in Sec. 12.8. Deal properly and explicitly with the issues of subtractions and of the necessary Ward identities in non-abelian gauge theories.

12.6 Obtain explicit factorization formulae for the differential cross sections for more complicated inclusive cross sections, e.g., $e^+ + e^- \to H_1 + H_2 + X$, $e^+ + e^- \to H_1 + H_2 + H_3 + X$. Assume here that the observed hadrons are at wide angles with respect to each other (and are not close to back-to-back in the two-hadron case). More general situations can be considered, of course. But that will lead you into other topics, such as those in Ch. 13.

12.7 Check and complete the one-loop calculations in Sec. 12.10.

12.8 Complete the one-loop calculations in Sec. 12.11. Verify that your results agree with Rijken and van Neerven (1997).